May 2014

Combined Metal-Enhanced Fluorescence-Surface Acoustic Wave (MEF-SAW) Biosensor

Samuel Morrill
University of South Florida, smorrill@jubii.dk

Combined Metal-Enhanced Fluorescence-Surface Acoustic Wave (MEF-SAW) Biosensor

by

Samuel Morrill

A thesis submitted in partial fulfillment
of the requirements for the degree of
Master of Science in Chemical Engineering
Department of Chemical and Biomedical Engineering
College of Engineering
University of South Florida

Major Professor: Venkat Bhethanabotla, Ph.D.
Robert Frisina, Ph.D.
Byeong Cha, Ph.D.

Date of Approval:
March 17, 2014

Keywords: Micro-mixing, removal, nanoparticles, immunofluorescence, bioassay

DEDICATION

I dedicate this work to my parents for always encouraging me to further my education no matter what as well as always being available to help when I was in need of anything. I would also like to dedicate this manuscript to my “second family” for always being there to lighten the mood and ensure this project never overwhelmed me.

ACKNOWLEDGMENTS

First, I would like to acknowledge my major professor, Dr. Venkat Bhethanabotla, for providing me with the guidance and the environment I needed to succeed. I would also like to acknowledge Debosruti Dutta for helping me understand many principles and for working with me on FDTD Solutions, as well as Mandek Richardson, for fabricating and helping me run SAW experiments as well as helping me understand many of the principles of immunohistochemistry. Also, special thanks to Jon Pickering for successfully making the nanoparticles used in this work.

Outside of my lab, I would like to acknowledge Dr. Byeong Cha from the Lisa Muma Weitz Advanced Microscopy and Cell Imaging Core Laboratory for help with imaging and immunofluorescence protocol. Also, thanks to Dr. Robert Frisina for allowing me to use certain features of his lab to improve my work.

TABLE OF CONTENTS

LIST OF TABLES

LIST OF FIGURES

ABSTRACT

Immunofluorescence assays are capable of both detecting the amount of a protein and the location of the protein within a cell or tissue section. Unfortunately, the traditional technique is not capable of detecting concentrations on the nanoscale. Also, the technique suffers from non-specific attachment, which can cause false-positives, as well as photobleaching when detecting lower concentrations is attempted. There is also a time constraint problem since the technique can take from many hours to a few days in some cases.

In this work, metal-enhanced fluorescence (MEF) is used to lower the detection limit and reduce photobleaching. Unfortunately, MEF also increases the intensity of non-specifically bound proteins (NSBPs). Therefore, a surface acoustic wave (SAW) device is used to remove the more weakly bound NSBPs. Previously, this has been shown on lithium niobate, but it is used with a quartz substrate in this work. The SAW device is also used to cause micro-mixing which speeds the process up significantly.

In this research, it was found that silver nanocubes can lower the detection limit down to below 1 ng/mL. Quartz SAW devices are shown to remove NSBPs at a power of 10 mW applied for five minutes. Micro-mixing is shown to be improved by a factor of six at 10 mW for 10 minutes by saturating the antibody used in this research, which takes 1 hour without micro-mixing. Finally, all three components are combined. In this work, the whole device is used to detect 50 ng/mL. After micro-mixing, the intensity is the same as with MEF, and, after removal, it has been lowered by 7 a.u.

CHAPTER 1: INTRODUCTION

Immunofluorescence (IF) assaying is a widely used technique for the detection of proteins and antigens/antibodies. The technique is highly adept at localizing antigens in either subcellular compartments or tissue sections, and, because it can map the actual location of antigens, it is highly useful for relating molecular architecture with the overall gross anatomy.[1]

There are some major problems with the immunofluorescence technique, however. For one, the fluorescence signal needs to be stronger. According to *Kuby Immunology*, IF is only capable of detecting concentrations down to 1 μg/mL and no further.[1] Many different methods have been used over the last couple of years to improve the fluorescence intensity. Recently, the use of metal nanoparticles of certain compositions of elements has been shown to cause fluorescence intensity enhancement of various fluorophores. The composition and the elements depend on the fluorophore signal wavelength that is desired to be increased. By overlapping the excitation/absorption spectrum of the fluorophore with the plasmonic peak of the nanoparticles, the fluorophore intensity can be increased significantly[2-13].

These metal nanoparticles also help fix another problem commonly encountered with immunofluorescence. Photobleaching is the "photochemical destruction of a fluorophore" that happens when reactive oxygen species are generated as a byproduct of the fluorescence excitation.[14,15] The longer the lifetime of the fluorophore, the more likely photobleaching is to occur. Fortunately, the addition of metal nanoparticles causes the lifetime to go down, decreasing photobleaching.[14,15]

Another problem with immunofluorescence is that biofouling in the form of contaminants affect the signal and produce background "noise" that makes the technique less efficient. On top of this, other antibodies and antigens affect the signal due to overlapping emission and excitation spectrums due in part to autofluorescence.[14,15] These antibodies and antigens are known as non-specifically bound proteins (NSBPs) and need to be removed, especially when trying to detect lower concentrations. To fix this problem, a SAW device can be used. Previously, Cular et al. have shown a SAW device on 128° YX lithium niobate chip can remove NSBPs as well as contaminants from biofouling.[16] This work has been redone in this thesis with a few key differences. For one, a quartz substrate is used as a novel substrate for removal. Another key difference is that the SAW device contains metal nanoparticles on its surface which need to be attached strongly enough to not be removed by the SAW energy.

Previously, Meyer et al. showed nonspecific binding removal using thickness shear mode resonators. In their work, quartz crystal resonators were used, and they managed to removed 85% of the nonspecifically bound protein.[17]

The final problem with immunofluorescence assays that an MEF-SAW device can improve is the amount of time required to complete the process. Getting the antibodies and antigens to attach to the desired surface can take a lot of time depending on the transport properties of the solutions being used. A SAW device can cause acoustic streaming making the proteins move faster through liquid vibration and therefore attach faster. This liquid vibration was first shown by Miyamoto et al. in 2002.[18] Then, in 2008, Paxton et al. showed this mechanism as a method for micro-mixing by doing plutonium uptake. They showed the SAW device enhancing the system by a factor of 5.8 times.[19] Normally, the incubation time for a secondary antibody is somewhere between two and four hours. Depending on the scheme, a

capture antibody may be needed as well. The attachment of the protein/antigen also takes a lot of time. With acoustic streaming, a process previously taking between hours and days can be reduced to minutes. The key to all of this is to be able to do this while not affecting the silver nanoparticles that will cause MEF. This is important because it has previously been shown that a SAW can remove nanoparticles.[20]

Metal-enhanced fluorescence (MEF), removal of NSBPs and biofouling on a lithium niobate SAW device, and mixing due to acoustic streaming have all been shown in separate experiments.[2-13,16,19] The novelty of this work is the combination of the SAW device with the MEF technique to improve the overall immunofluorescence assay as well as the use of quartz as the SAW piezoelectric material instead of lithium niobate.

In Chapter 2 of this thesis, protein detection schemes that have previously and that are currently being used will be described. Most of the information in this chapter comes from the seventh edition of *Kuby Immunology*. The last section describes what *Kuby Immunology* has to say about immunofluorescence.[1]

In the following chapters, all of the work that has been done will be described. The first experiments performed dealt with Metal-Enhanced Fluorescence by itself. In this section, experimental work to first show MEF was performed. Then, the usage of MEF for actual detection was performed. In this section, theoretical work associated with MEF is also described.

In Chapter 4, removal of non-specifically bound proteins is explored. Also in this section, the possibility of removing specifically bound proteins as a method to restore and recycle devices is briefly explored.

In Chapter 5, micro-mixing with the SAW device is described. In the work in this section, nanoparticles still have not been added to the procedure and only mixing is actually considered.

Finally, in Chapter 6, the device utilizing MEF, removal, and mixing as an all-in-one package is described. In this chapter, the work showing all three components can co-exist is described. Final conclusions about the device are also discussed at the end of this chapter.

In the Appendices, all of the images and graphs that could not be included in the body of work can be seen.

CHAPTER 2: CURRENT DETECTION TECHNIQUES

Immunoassays are currently the predominant method for detecting proteins. In particular, ELISA is the preferred method for doing this. Compared to most other assays, ELISA has a fairly good sensitivity of 0.0001-0.01 µg of protein per milliliter of sample and even below in some cases.[1] Some other assays also used include precipitation reactions, agglutination reactions, radioimmunoassay, flow cytometry, western blotting, and immunofluorescence.[1] In this chapter, most of the techniques and assays that have been and currently are used to detect proteins will be summarized. The effectiveness will be described as will its usefulness for detecting biomarkers which can require low detection limits as well as time and cost associated with the technique. In the last section of this chapter, the traditional way immunofluorescence is done will be described. Most of the information for this chapter comes from *Kuby Immunology*.

2.1 Sensing with Precipitation Reactions

Sensing with precipitation reactions is based on the principle that a soluble antigen and a precipitating antibody together in a gel or liquid medium will form an antigen-antibody precipitate. One major problem with this is that the formation of the precipitate takes as long as one to two days depending on the valency of the antibody and antigen. Another issue is that the antibody has to be bivalent while the antigen must be either bivalent or polyvalent. The main issue, however, is the low sensitivity of the method requiring a large amount of sample to be used. Table 2-1 below shows the sensitivities of various precipitation reaction processes.[1]

Thermo Scientific describes a Lowry Protein Assay that uses a precipitation reaction to detect proteins. The assay is made using copper chelation chemistry.[21] This method does appear a little bit faster, but it does not mention the sensitivity which likely means that the detection limit is not any lower than those mentioned in *Kuby Immunology*.

Table 2-1. Sensitivities of some sensing methods using precipitation reactions. Data from *Kuby Immunology*.[1]

Assay	Sensitivity (µg antibody/mL)
Precipitation reactions in fluids	20-200
Precipitation reactions in gels	
Mancini radial immunodiffusion	10-50
Ouchterlony double immunodiffusion	20-200
Immunoelectrophoresis	20-200
Rocket electrophoresis	2

Precipitation reactions are done in either a fluid medium or a gel medium. In the fluid medium, plotting the amount of precipitate formed versus the increasing antigen concentration will result in what is called a precipitin curve. Then, excess antigen and excess antibody can be used to analyze the data.[1]

In the gel medium, there are a number of different methods possible. These methods result in visible precipitin lines. The Mancini method and the Ouchterlony method use immunodiffusion to form precipitin rings. By measuring the area of the ring and comparing it to a standard curve, the antigen concentration can then be determined. Immunoelectrophoresis combines electrophoresis with immunodiffusion. This method has been useful in identifying immunodeficiency diseases. Lastly, rocket electrophoresis is a quantitative technique that can measure antigen levels. The precipitate is shaped like a rocket after negatively charged antigen is electrophoresed in a gel with antibody. This technique is more sensitive than the other precipitation reaction techniques.[1]

Compared to other sensing techniques, this technique is extremely bad sensitivity-wise. Combined with the fact that it can take one or two days to complete, the technique is not nearly as useful as a method for many biomarkers anymore.

2.2 Sensing with Agglutination Reactions

The interaction between some antibodies and antigens results in visible clumping that is known as agglutination. Only some antibodies cause this, and they are called agglutinins. Agglutination reactions depend on the crosslinking of polyvalent antigens. In these reactions, inhibition due to excess antibody is known as the prozone effect.[1] This inhibition resembles the one that causes excess antibody in precipitation reactions.

Agglutination reactions are much more effective today than precipitation reactions. By using synthetic beads as the matrix for the reactions instead of red blood cells, the process can be as short as three to five minutes. Also, the techniques for this are much more sensitive than precipitation reactions as can be seen in Table 2-2.[1] For these reasons, the technique is still used in blood typing and to diagnose infections.[1] However, the sensitivity is not good enough for the technique to be useful for most biomarkers. At a minimum detection of 6 ng/mL, biomarkers concentrations below this level cannot be accurately determined. Currently, the technique can detect lower concentrations that traditional immunofluorescence can. It does not approach the possibilities of ELISA, however.

Table 2-2. Sensitivities of agglutination reactions. Data from *Kuby Immunology*.[1]

Agglutination reactions	Sensitivity (µg antibody/ml)
Direct	0.3
Passive	0.006-0.06
Inhibition	0.006-0.06

2.3 Radioimmunoassay

Radioimmunoassay (RIA) is one of the most sensitive antigen or antibody sensing techniques currently in use. The technique is capable of sensing levels as low as 0.0006-0.006 μg antibody per milliliter.[1]

The technique was first utilized in 1960 by Berson and Yalow to assay for insulin concentration in plasma. Fifty years later, it is still being used in blood banking, diagnosis of allergies, and endocrinology among others.[22]

In RIA, radiolabeled antigen is competitively bound to a high-affinity antibody until saturation is reached. Then, unlabeled antigen is added to compete for binding sites. The decrease in radiolabeled antigen is then measured to determine how much antigen is present. By using different concentrations of unlabeled antigen, a curve can be generated to determine the amount of antigen left in the mixture.[1] Figure 2-1, taken from *Kuby Immunology*, shows how this method works when detecting Hepatitis B.

The technique is widely used due to its great sensitivity. Of course, a radioactive technique does have some drawbacks. The expenses and hazards associated with the preparation and handling of radioactive antigen is great. Measuring gamma radiation requires special counting equipment which is also expensive. Also, radioactive iodine atoms concentrate in the thyroid gland affecting the signals.

Despite the drawbacks, RIA is a major factor in the measuring of plasma levels for most hormones, some abused drugs, and digitoxin or digoxin for patients receiving hormones. It is also used to look for hepatitis B in donated blood and anti-DNA antibodies in systemic lupus erythematosus.[22] The overall technique is similar to immunofluorescence. Instead of a fluorescence label, a radioactive label is used. Also, instead of using a fluorescence microscope

to do the imaging, equipment for radioactivity is used. However, RIA is much more effective while also much more dangerous.

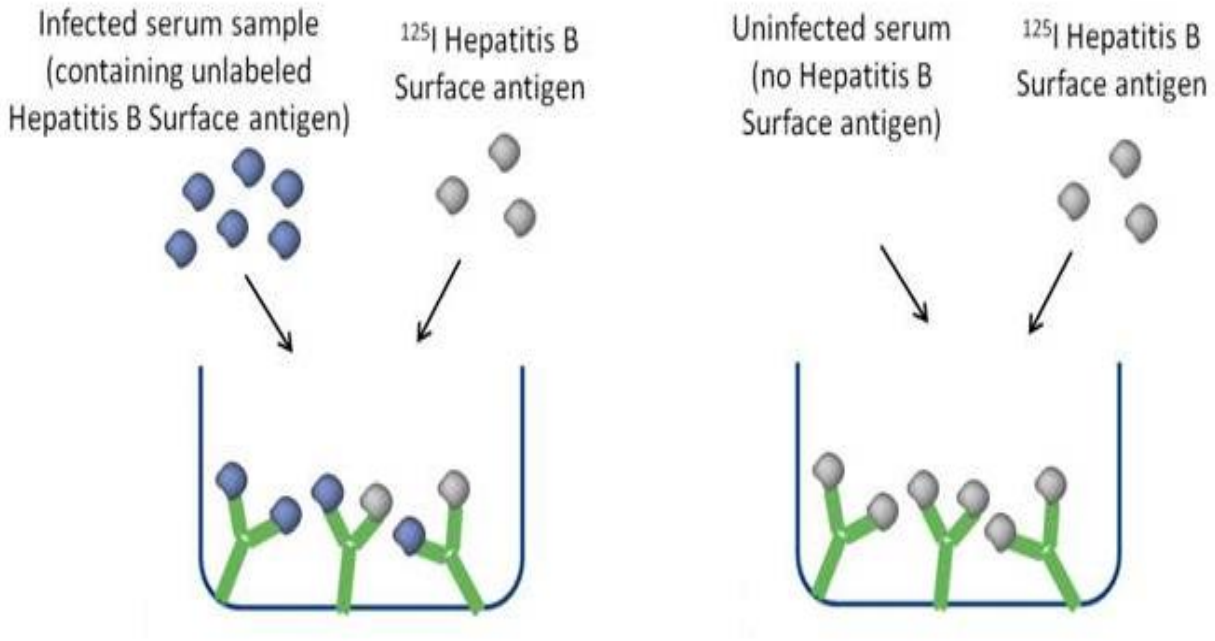

Figure 2-1. Using RIA to detect hepatitis B in blood.[23] Microtiter wells are coated with antibody that is specific for the hepatitis B antigen. Then, the infected blood is added followed by the uninfected blood.

2.4 ELISA

Enzyme-linked immunosorbent assays (ELISAs) are designed to detect and quantify substances such as antibodies, proteins, peptides, and hormones.[24] The detection is done by "assessing the conjugated enzyme activity via incubation with a substrate to produce a measurable product." This is highly dependent on the specificity of the antibody-antigen interaction.[24]

ELISA depends on an enzyme conjugated with an antibody which reacts with a colorless substrate and generates a colored reaction product. Some of the enzymes that are employed include "alkaline phosphatase, horseradish peroxidase, and β–galactosidase."[1] Overall, it is a

safer process and less costly than a technique such as radioimmunoassay, while also improving on the sensitivity of radioimmunoassay.[1]

Many different techniques and variations of ELISA have been developed over the years. Three variants are indirect ELISA, sandwich ELISA, and competitive ELISA. These techniques are all similar and the classification essentially depends on the order and ways in which the antigens/antibodies are added. Indirect ELISA is currently the most common technique for identifying HIV[1], and this technique is shown in Figure 2-2.

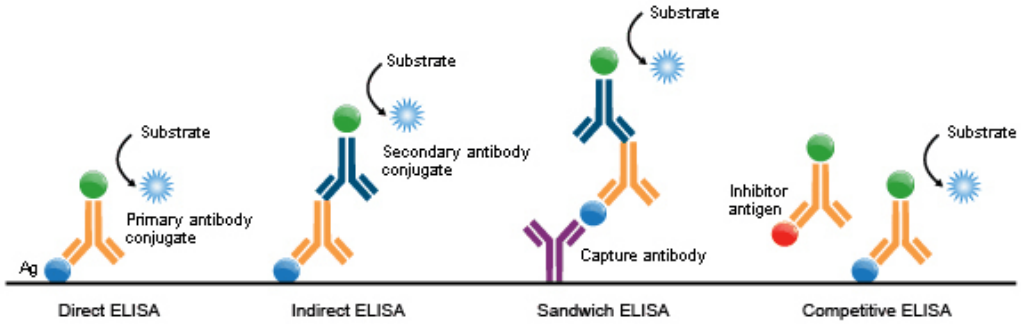

Figure 2-2. Illustration of different ELISA techniques.[25]

Another way to do ELISA is via chemiluminescence. This works by measuring light intensity during certain chemical reactions instead of measuring absorbance like the previous methods do.[1]

There is also the ELISPOT assay which is a modification on ELISA that allows you to quantitatively determine how many cells are producing antibodies specific for an antigen. This works as a sandwich assay by capturing proteins locally as they are secreted. The detection is then done by a precipitating substrate. It is similar to a Western blot.[24]

In-cell ELISA is yet another variant. This is cultured overnight and, once the cells are fixed, permeabilized, and blocked, antibodies are used to detect the target proteins. This technique works as an indirect assay.[24]

As with other techniques that have many variants, there are positives and negatives to each variation. Direct ELISA detection is quick because it uses only one antibody and requires fewer steps. This also eliminates cross-reactivity of secondary antibody. Indirect ELISA uses a wide variety of commercially available secondary antibodies and is very versatile due to this. The immunoreactivity is at a maximum since labeling does not take any available attachmetns and is therefore more sensitive as well.[24]

On the other hand, direct ELISA detection can adversely affect immunoreactivity, requires time-consuming and expensive primary antibody labeling, has little signal amplification, and is inflexible. For indirect ELISA, cross-reactivity is a significant problem, and it also takes longer because an extra incubation step is required.[24]

2.5 Western Blotting

Western blotting is a good process for identifying a specific protein in a mix of many proteins. It does this by allowing the researchers to determine the molecular weight of the target protein and thereby be able to calculate the amount of the protein in the sample.[26]

First, the mixture is treated with sodium dodecyl sulfate (SDS) which is a strong denaturing agent. The mixture is then separated via electrophoresis in an SDS polyacrylamide gel which is capable of separating components based on molecular weight. The proteins in the gel are then treated with a sheet of nitrocellulose or nylon which acts as a protein-binding sheet causing the proteins to attach to the sheet due to electric current. Enzyme-linked antibodies can then detect the antigen desired and position is realized through an ELISA reaction. *Kuby Immunology* provides a great schematic for how this process works and this is shown in Figure 2-3.

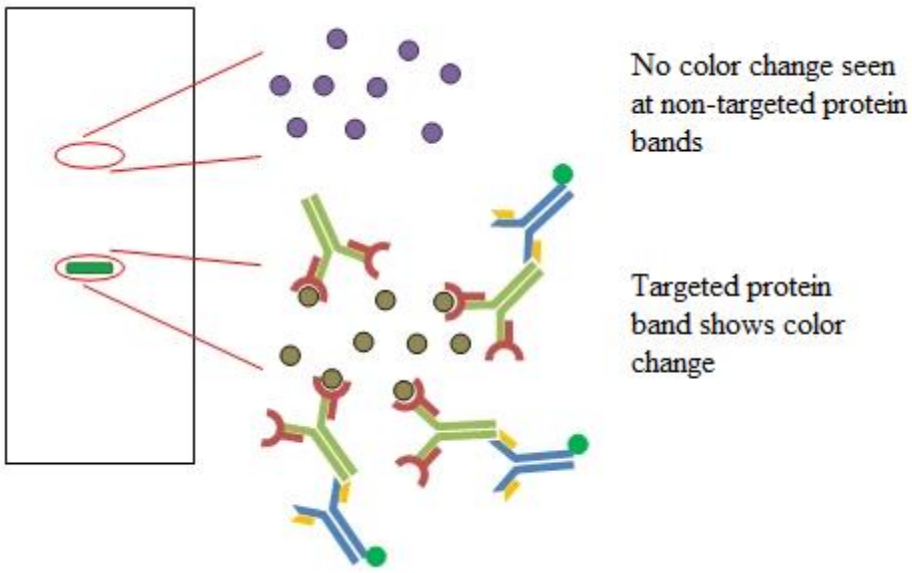

Figure 2-3. Western Blotting technique.[27]

2.6 Immunoprecipitation

This technique allows for isolation of the desired antigen. By mixing the antigen solution with antibody, antibody-antigen complexes precipitate out. It can then be determined if an antigen is actually synthesized by a cell or tissue. The problem with this technique is that it can take hours or days for the precipitate to form unless additional techniques including centrifugation are used.

Immunoprecipitation works very much in conjunction with other protein detection schemes. According to Thermo Scientific, it is used to "investigate the presence, relative abundance, size, up-regulation, stability, post-translational modification, and interaction of proteins." The protein that comes from the technique can then be analyzed using other methods like ELISA or Western blotting to quantify the proteins.[28]

Just like other methods mentioned in this chapter, there are multiple variations of the technique. Immunoprecipitation (IP), Co-Immunoprecipitation (Co-IP), and Pull-Down assays

are all variations with different strengths and weaknesses.[28] The technique to be used depends on what it is being used for.

2.7 Flow Cytometry

Flow cytometry allows for quantitative data that is not possible with other techniques. A laser beam is used to excite fluorophores, and light detectors are used to measure the intensity of the emission from the fluorophores. Every time a cell attached with a fluorophore passes through the laser beam, excitation occurs and light is deflected from a first detector. A second detector then records the intensity of the emitted light.[1]

The method allows for a lot of information to be obtained. It can determine a quantitative number of cells expressing the target antigen, the antigen density in the sample, and the size of the cells. It is also possible to flow through multiple antibodies with different fluorophores expressing different colors at the same time.[1]

According to Kuby Immunology, the method has about the same sensitivity as the agglutination reaction methods. Its sensitivity is measured at around 0.006-0.06 µg antibody per milliliter of solution.[1] This is better than normal immunofluorescence but much worse than ELISA.

Figure 2-4. Flow cytometer from BD Accuri.[29]

2.8 Sensing without Antigen-Antibody Reactions

In the cell walls of some strains of *Staphylococcus aureus*, a molecule known as protein A is present. In the walls of group C and G Streptococcus, protein G is present. By combining protein A and G, a recombinant protein called protein A/G can be made which has the best features of both proteins. This protein is useful because it binds many forms of IgG. By labeling protein A/G with radioactivity, biotin, or fluorochromes, IgG formed during ELISA, RIA, or fluorescence experiments can be detected.[1]

Another method comes by using streptavidin due to its high affinity and specificity for biotin. The antibody can be labeled with biotin, react with the antigen, and then wash away the unattached antibody. Then, a conjugated enzyme, fluorochrome, or radioactive label can be detected.[1]

2.9 Immunoelectron Microscopy

An electron-dense label can be conjugated to the Fc region of a specific antibody either directly or indirectly. *Ferritin* and *colloidal gold* are two examples of labels used. These labels will absorb electrons which results in black dots when using the electron microscope. This allows for the identification of many antigens by identifying the sizes of the label particles.[1]

2.10 Immunofluorescence

A useful discovery by Albert Coons was that antibodies can be labeled with fluorophores. A fluorophore is a compound that can emit light at a certain wavelength after getting excited at another wavelength. Once tagged with the fluorophore, a fluorescence microscope can be used to see the location of the antibody.

There are some problems with this technique. The signal from the fluorophores often is not strong enough. Also, background "noise" or signals affect the clarity of the image. The overall technique also takes a fairly long time to take place because of the time it takes for the antigens to attach to the antibodies. The goal of this thesis is to create a device to solve these problems and make this a technique that can compete with ELISA.

Kuby Immunology states that immunofluorescence only has a sensitivity of 1 µg of antibody per milliliter. Immediately, the purpose of the MEF is shown. Robinson et al. mention photobleaching problems with immunofluorescence.[15] This is yet another reason to utilize MEF. MEF will cause the sensitivity to get better while removing the photobleaching effects.

Robinson et al. also mention autofluorescence and fluorescence overlap as major problems for immunofluorescence.[15] Fortunately, this is where the SAW device will be able to help by removing these phenomena to some extent. On top of that, the SAW device will be able to shorten the procedure from a matter to hours to a matter of minutes.

Traditionally, the technique works as follows. An attachment layer is placed on the substrate, which is normally glass. Then, the cell of interest or protein/antigen is attached to the adhesion layers. There are two methods that can be used from this point. Direct immunofluorescence attaches an antibody directly tagged with fluorophore which is followed by imaging. Indirect fluorescence first attaches an antibody without a fluorophore and then follows with a secondary antibody that is tagged with fluorophore. Indirect fluorescence is more expensive and takes longer, but it is more sensitive due to more attachment sites.[1]

The method proposed in this work is similar to direct immunofluorescence. However, a capture antibody is required so that removal can be done. Also, the nanoparticles are attached strongly so that MEF and removal/micro-mixing can be done simultaneously.

Figure 2-5 is a simple representation of normal immunofluorescence procedures. In this diagram, direct and indirect immunofluorescence can be seen.

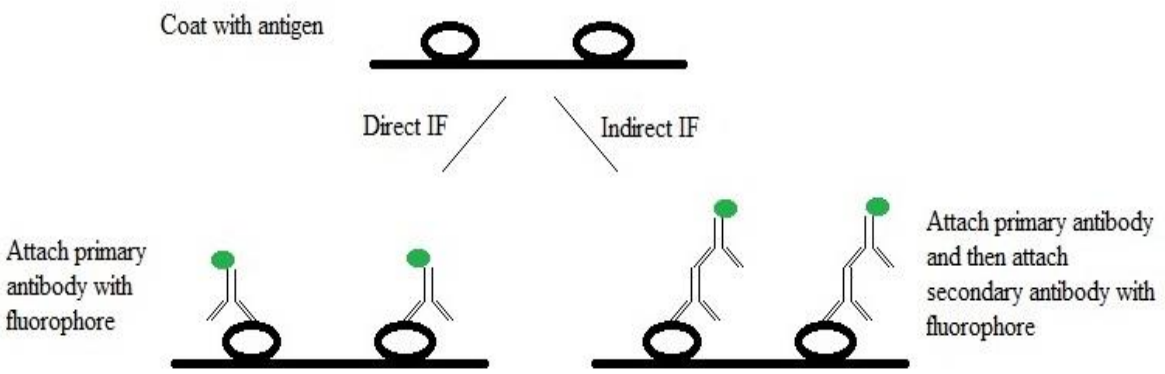

Figure 2-5. Traditional immunofluorescence techniques.

CHAPTER 3: METAL-ENHANCED FLUORESCENCE

The ability of nanoparticles and nanostructures with many diverse characteristics to cause enhancement of fluorescence has been well-documented on many different substrates in recent years. All the way back in 2002, Lakowicz et al. and Gryczynski et al., working together, were showing enhancements in the single digits but potentially much higher using silver island films.[8,10] Since then, many different methods have been used to improve the enhancement. For instance, seven years later, in 2009, Chowdhury et al. showed much greater enhancement on glass using two extremely different methods. They sputtered silver-copper nanostructures on glass surfaces and measured enhancements for Alexa Fluor 488 and Alexa Fluor 594 as high as 141.48±19.20 and 23.91±12.37 times, respectively.[3] In another method, they synthesized spherical silver-copper bimetallic nanoparticles and managed to show an enhancement as high as 55.33±15.23 times when the ratio of silver to copper was 2:1. Also, when the ratio went higher in favor of copper, the enhancement steadily decreased.[4] Progress continues to be made.

Many more examples of nanostructures showing enhancement can be found throughout literature. It has not been shown working in conjunction with a SAW device made out of materials such as lithium niobate or quartz, however. If metal-enhanced fluorescence is possible on the lithium niobate surface or the quartz surface, then the advantages of the SAW device can be used together with MEF. This overall device could result in a better way to do immunofluorescence techniques that, depending on the magnitude of the enhancement and the

effect of the SAW device, can be much more effective than regular immunofluorescence assays currently in use.

3.1 Origin of MEF

The interaction between light and noble metal nanoparticles has been studied extensively since Michael Faraday noticed the ruby-red color emission from colloidal gold as far back as the mid-1800s. This happens because nanoparticles are able to support surface plasmons, which are collective oscillations of conduction electrons. The wavelength of the plasmons' oscillations changes depending on the characteristics of the nanoparticle such as the size, shape, material, and surrounding environment of the nanoparticle.[11]

Metal-enhanced fluorescence (MEF), also known as surface-enhanced fluorescence (SEF), was first discovered four decades ago when Drexhage et al. showed alteration of the fluorescence of an Eu^{3+} complex due to a flat metallic surface.[11] Many different studies have shown the effect to varying degrees since this discovery. The fluorescence emission is enhanced due to a strong local field that is near the metal surface because the surface plasmons are being excited by the light. Through the interaction of the fluorophore molecule with the metal surface, decay rates for the fluorophore are altered which leads to fluorescence enhancement.[11]

As described by Morton et al., a molecule's fluorescence efficiency is typically expressed through a term known as the fluorescence quantum efficiency, Φ^{FQE}, which is calculated by

$$\boldsymbol{\Phi^{FQE}} = \frac{\boldsymbol{\gamma}}{\boldsymbol{\Gamma}} \tag{1}$$

where γ is equal to the free molecule radiative transition rate and Γ is equal to the overall decay rate.[11] According to Fermi's golden rule, the equation for γ is given by

$$\boldsymbol{\Phi}\gamma = \frac{2\pi}{\hbar}\left|\mu_{eg}\right|^2 \rho_g \tag{2}$$

In equation (2), μ_{eg} is the transition dipole moment between the electronic excited state, denoted as *e*, and the ground state, denoted by *g*, while ρ_g is defined as the density of photons at the ground state.[11] Meanwhile, in equation (1), the overall decay rate, Γ, is given by

$$\Gamma = \gamma + k_{nr} + k_{int} + k_{pc} \quad (3)$$

In this equation, all the *k* terms are the nonradiative transitions while γ is the radiative transition. In equation (3), k_{nr} is the nonradiative decay rate due to thermal, collisional and vibrational losses, k_{pc} is the rate of photochemical processes such as irreversible photobleaching, and k_{int} is the rate of internal conversion which is usually so fast that it can be ignored in the equation.[11]

The addition of certain metals to these systems can affect the equations in numerous ways. According to Garoff et al., the radiative decay rate is affected by a multiplicative enhancement while the nonradiative decay rate is an additive enhancement. This changes equation (3) into

$$\Gamma = \gamma|E(\omega', r)|^2 + k_{nr} + k_{pc} + k_M \quad (4)$$

where the new term $|E(\omega',r)|^2$ is an electric field enhancement factor at the metal-molecule distance r and the emission frequency ω'. The other new term, k_M, is the nonradiative decay caused by the metal.[30] Overall, the MEF is caused by these two new terms.

The interesting thing here is that the presence of the metal will increase the fluorescence quantum efficiency toward one while also decreasing the lifetime τ (equal to the inverse of the overall decay rate). In conventional fluorescence, the lifetime would increase with increasing fluorescence quantum efficiency which is a problem because more photobleaching would happen. With the metal addition, however, this is no longer a problem.[11]

These facts can be more clearly illustrated when considering the equations for quantum yield (Q_0) and fluorophore lifetime (τ_0). The quantum yield is defined as the number of emitted

photons per absorbed photon, while the lifetime is the amount of time it takes for an excited photon to return to the ground state. Without a metal, these equations are:[7]

$$Q_0 = \frac{\Gamma}{\Gamma + k_{nr}} \tag{5}$$

$$\tau_0 = \frac{1}{\Gamma + k_{nr}} \tag{6}$$

When the metal is added, these equations become:

$$Q_M = \frac{\Gamma + \Gamma_M}{\Gamma + \Gamma_M + k_{nr}} \tag{7}$$

$$\tau_M = \frac{1}{\Gamma + \Gamma_M + k_{nr}} \tag{8}$$

In equations (7) and (8), the added Γ_M term is the radiative decay rate due to the presence of the metal.[7]

These four equations clearly show why the quantum yield will increase and the fluorophore lifetime will decrease. In equation (7), as Γ_M approaches infinity, Q_M will approach one. When Γ_M approaches infinity in equation (8), τ_M will approach zero.

Altogether, the excitation of the plasmons leads to a higher excitation of the electrons in the fluorescent molecule when the absorbance of the metal nanoparticles lines up with the excitation spectrum of the fluorophore. When more electrons are excited, more emission of light will occur resulting in an intensified fluorescence signal.

3.2 Plasmonics

The field of study on the abilities of metal nanostructures and nanoparticles to manipulate light at the nanoscale is called plasmonics.[31] The MEF phenomenon is a subtopic in this broad field, along with other topics such as Surface-Enhanced Raman Scattering (SERS). Recent

advances in the synthesis, assembly, characterization, and theory of metal nanostructures has led to huge advancements in fields including sensing, therapeutics, and photovoltaics.[31]

3.2.1 Localized Surface Plasmon Resonance (LSPR)

Localized Surface Plasmon Resonance is a subfield of plasmonics that is associated with resonances due to noble metal nanostructures which cause spectral absorption, scattering peaks, and strong electromagnetic near-field enhancements. A plasmon is essentially a collective oscillation of free electrons in noble metals. The oscillations occur at the plasma frequency with energy:[32]

$$E_p = \hbar\sqrt{\frac{ne^2}{m\varepsilon_0}} \tag{9}$$

In equation (9), ε_0 is the permittivity of free space, n is the electron density, e is the electron charge, and m is the electron mass.[32]

Surface plasmons, also known as surface plasmon polaritons (SPP), form at the metal-free space interface, and they can be optically excited by coupling of light through a grating defect in the metal. When the noble metal nanoparticles are of the same dimensions as the wavelength of light, free electrons participate in the excitation and cause localized surface plasmon (LSP). This effect enhances local electric fields.[32]

To understand this phenomenon, Mie theory was developed in the early 20th century by Gustav Mie. He developed an analytical solution for the scattering and absorption of light by spherical particles. Unfortunately, other nanoparticle forms cannot be solved analytically and need to be solved numerically.

Mie found that for extremely small particles that are much smaller than the wavelength of light, the scattering is similar to Rayleigh scattering. By defining the sample as a plane wave

incident on a homogeneous conduction sphere, the scattering, extinction, and absorption cross sections can be solved:[32]

$$\sigma_{sca} = \frac{2\pi}{|k|^2}\sum_{L=1}^{\infty}(2L+1)(|a_L|^2 + |b_L|^2) \quad (10)$$

$$\sigma_{ext} = \frac{2\pi}{|k|^2}\sum_{L=1}^{\infty}(2L+1)[Re(a_L + b_L)] \quad (11)$$

$$\sigma_{abs} = \sigma_{ext} - \sigma_{sca} \quad (12)$$

For equations (10)-(12), k is the incoming wavevector and L is all the integers representing dipole, quadrupole, and higher and higher multipoles of scattering. a_L and b_L can be represented using the Riccati-Bessel functions ψ_L and χ_L:[32]

$$a_L = \frac{m\psi_L(mx)\psi_L'(x) - \psi_L'(x)\psi_L(x)}{m\psi_L(mx)\chi_L'(x) - \psi_L'(mx)\chi_L(x)} \quad (13)$$

$$b_L = \frac{\psi_L(mx)\psi_L'(x) - m\psi_L'(mx)\psi_L(x)}{\psi_L(mx)\chi_L'(x) - m\psi_L'(mx)\chi_L(x)}) \quad (14)$$

In equations (13) and (14):

$$m = \frac{\tilde{n}}{n_m} \quad (15)$$

$$x = k_m r \quad (16)$$

In equation (15), this is equal to the refractive index of the material divided by the refractive index of the surrounding material and the refractive index of the material can be defined as:

$$\tilde{n} = n_R + in_I \quad (17)$$

Also, in equation (16), r is the radius of the metal particle while k_m is the wavenumber in the medium.[32]

These equations are difficult to solve. However, by assuming that x, defined in equation (16), is much smaller than 1, Mie realized that the Riccati Bessel functions can be approximated using a power series and keeping terms to x^3. Doing this, equations (13) and (14) become:

$$a_1 \approx -\frac{i2x^3}{3}\frac{m^2-1}{m^2+2} \tag{18}$$

$$b_1 \approx 0 \tag{19}$$

With some more mathematical manipulation, equations (10) and (11) can become:

$$\sigma_{sca} = \frac{32\pi^4 {\varepsilon_m}^2 V^2}{\lambda^4}\frac{(\varepsilon_1-\varepsilon_m)^2+(\varepsilon_2)^2}{(\varepsilon_1+2\varepsilon_m)^2+(\varepsilon_2)^2} \tag{20}$$

$$\sigma_{ext} = \frac{18\pi {\varepsilon_m}^{1.5} V}{\lambda}\frac{\varepsilon_2(\lambda)}{[\varepsilon_1(\lambda)+2\varepsilon_m]^2+\varepsilon_2(\lambda)^2} \tag{21}$$

As mentioned previously, these results are only valid for spherical nanoparticles. Also, the equations are only supposed to work for particle diameters below 10 nm, but it has been shown to be consistently successful for larger particles as well. To do different shapes, such as cubes, rods, or pyramids, numerical methods are required.[32]

3.3 Particle Size, Shape, and Material Effects

The characteristics of the nanostructures or nanoparticles have a high effect on the amount of enhancement of fluorescent molecules that will occur. Rahmani et al. used linear response theory mixed with coupled dipole approximation to find out that the largest enhancements occur in the areas with the most curvature.[11] It is also well-established that the size, the material of the metal used, and the surrounding environment is important in determining the amount of enhancement likely to occur for fluorophores.[32] The enhancement is dependent on the excitation peak of the fluorophore matching up with the plasmonic peak of the nanoparticles.

3.3.1 Size

Mie theory states that for spherical particles with a radius R that is much smaller than the wavelength of light, the scattering cross-section is proportional to R^6 while absorption is only

proportional to R^3. When the particles are smaller, the localized surface plasmon resonance (LSPR) is dominated by absorption. As the particle size increases, scattering begins to take over. For gold spheres, the transition from scattering dominance begins at a diameter of approximately 80 nm.[32]

Size also affects the LSPR wavelength. By changing the size of gold spheres from 10 to 100 nm, the LSPR wavelength can change by 60 nm. This is due to interband transitions contributing increased line width for small particles and higher plasmon modes contributing to increased line width in larger particles. By changing the size, the amount of LSPR occurring as well as where it occurs in the light spectrum can be greatly affected.[32]

3.3.2 Shape

As mentioned previously, to determine the effect of shape, numerical or experimental methods must be used because analytical ones cannot be solved. By increasing the sharpness and quantity of tips, resulting in higher curvature, the refractive index increases which results in a bigger LSPR effect. Many works have shown that other shapes have a stronger effect than spheres. Mock et al. showed that silver nanotriangles had a sensitivity around 350 nm/RIU while spheres only showed 160 nm/RIU. Also, Sun et a. showed gold nanoshells with a sensitivity of 409 nm/RIU while gold spheres only had 60 nm/RIU. The increase cannot be seen as just due to shape, however. The size, shape, and material all combine to affect how the LSPR effect happens.[32]

As with changing size, the plasmon resonance can be red-shifted by increasing the number of sharp tips. This is due to an increase in the refractive index sensitivity. Two numerical

methods that can be used to calculate the effect of various shapes are the finite difference time domain (FDTD) method and the finite element method (FEM).[32]

3.3.3 Material

Gold and silver are the primary noble metals used to make the plasmonic effect occur. While silver is able to give better resonance, gold is often used since it is chemically stable and resistant to oxidation. To display the effect of silver versus gold, consider the effect for 50-60 nm in diameter spheres made of either silver or gold. Silver is at 160 nm/RIU at a plasmon resonance around 435 nm while gold is at 60 nm/RIU at a resonance of about 530 nm. This difference is due to the dielectric functions of the two metals, which is dependent on the refractive index sensitivity. Silver varies more with wavelength than gold in the visible light region. Also, the imaginary part of silver's dielectric function is less than gold in the visible region so less damping happens. This results in narrower plasmons linewidths as well as higher scattering efficiency.[32]

3.3.4 Alloy Effect

Many people have done different studies on the effect that alloying metals can have on the plasmonic peak and the plasmonic resonance. Chowdhury et al. combined silver with copper in varying ratios both by sputtering and by the creation of alloy nanospheres. They found quenching with no silver and the maximum enhancement with no copper.[3,4] If one type of fluorophore is desired to be quenched, this could also be a useful discovery.

In another study, Golberg et al. created silver islands films (SIF) and combined them with aluminum. Using fluorescein, they did numerous studies and found that SIF combined with 8 nm

of aluminum was much more effective than SIFs or aluminum by itself.[7] Many other researchers have also used silver islands, but they don't appear as effective for this research. In this work, Alexa-488 was used which has similar properties to that of fluorescein.

3.4 Theoretical Work

FDTD Solutions was used to calculate the theoretical absorbance, scattering, and extinction spectra that can be expected for silver cubes from 10-90 nm edge dimensions. The refractive index of the surrounding environment was kept at 1.333 to represent a PBS environment. Theoretically, only the size was considered.

To calculate absorbance, scattering, and extinction, the set-up included a total field scattered field (TFSF) source in proximity to the nanoparticle. The material used was "Ag – Palik (0-2um)." The optical properties of this material were not measured specifically for silver cubes so some error is encountered. Particularly, the results show red-shift of approximately 50 nm. Then, after running the simulation, a script was used to calculate the absorbance, scattering, and extinction. The full scripts can be seen in Appendix B. The equations and definitions for terms for the three spectrum are shown in equations 22, 23, and 24.

$$Qabs = sigmaabs/(pi * aeff^2) \tag{22}$$

$$Qscat = sigmascat/(pi * aeff^2) \tag{23}$$

$$Qext = Qabs + Qscat \tag{24}$$

Figures 3-1, 3-2, and 3-3 show the differences in spectra based on size. As mentioned above, the graphs follow conventional knowledge, but they are shifted due to the optical properties of the silver. Only 30, 50, and 70 nm edges are shown here. The rest can be seen in Appendix B.

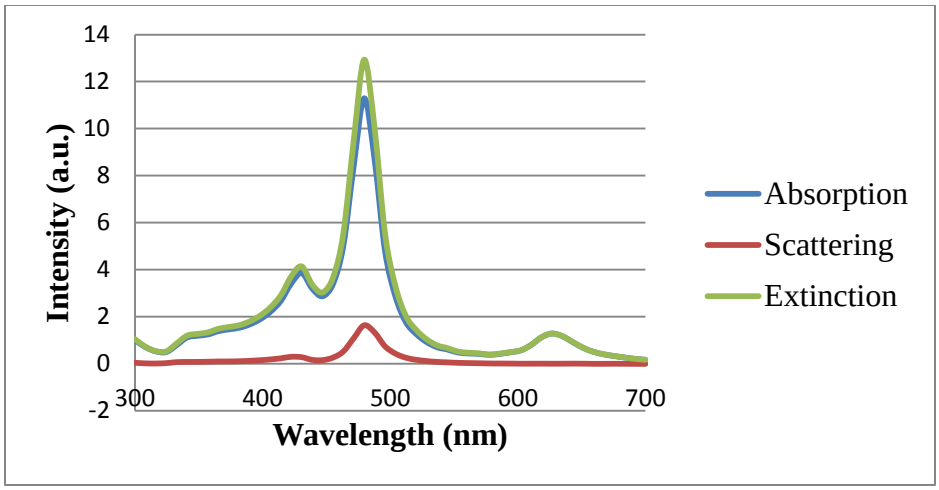

Figure 3-1. Absorption, scattering, and extinction spectra of nanocubes with 30 nm edges.

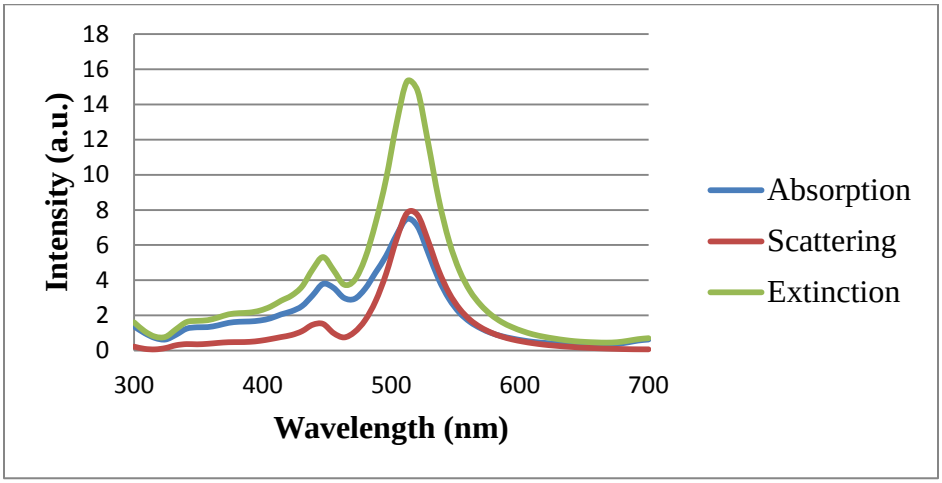

Figure 3-2. Absorption, scattering, and extinction spectra of nanocubes with 50 nm edges.

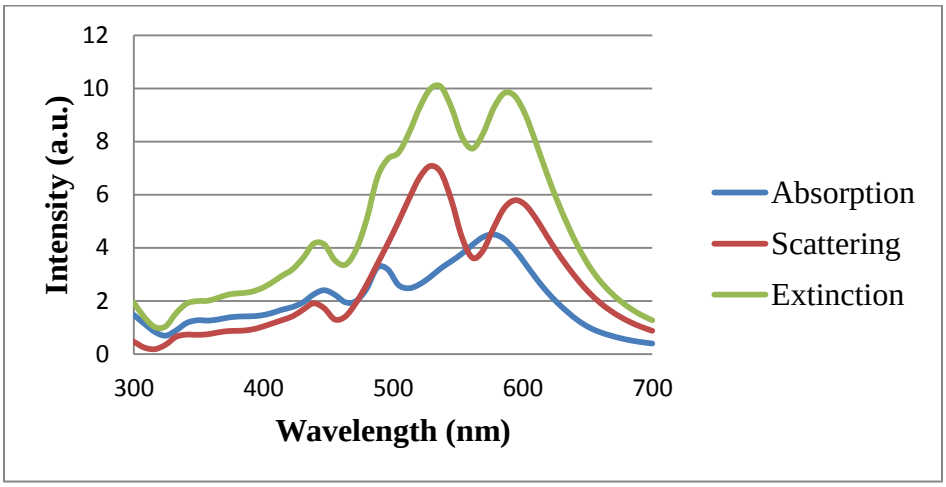

Figure 3-3. Absorption, scattering, and extinction spectra of nanocubes with 70 nm edges.

3.5 Experimental Procedure

A number of different experiments were performed to not only show MEF but to also use it to detect antigens. To show MEF, sputtering and nanoparticles were used. To detect with MEF, only nanoparticles were used. The materials used throughout all the experiments were normal rabbit IgG, goat anti-rabbit IgG tagged with Alexa-488 and phosphate buffer solution (PBS).

3.5.1 Sputtering to Cause MEF

A number of different approaches were taken to achieve metal-enhanced fluorescence. The simplest method involved sputtering of silver onto lithium niobate. Lithium niobate was required because peaks and curvature are the important aspects to create MEF. Glass has a different structure than lithium niobate so different size peaks would occur if sputtering were done on glass. Initially, the thought was that $LiNbO_3$ would be used as removal has already been proven on that substrate. After proving quartz could achieve the same effect, that substrate was used with nanoparticles.

Sputtering for 90 seconds with a current around 33 mA was found to be most effective at creating peaks, especially when using a higher pressure such as 9 mTorr. The machine used was a CRC sputterer. Atomic Force Microscopy (AFM) was used to determine the peaks achieved. At 180 seconds and the same conditions otherwise, the peaks were also present but smaller. When sputtering at 270 seconds and the same conditions, the peaks were less common but a few were still seen with AFM.

Once the silver was on the lithium niobate chip, antibody tagged with fluorophore needed to be attached to test for enhancement. Alexa-488 was the fluorophore used. It was attached to donkey anti-mouse IgG bought at 2 mg/mL from Invitrogen. This was diluted down to 10 µg/mL

using PBS. Then, 10 µL was applied to the surface of the silver. After incubating for 20 minutes, the surface was suctioned, rinsed with 10 µL of PBS three times, and imaged using a Leica DMI4000 B fluorescence microscope.

3.5.2 Nanocubes to Cause MEF

A more complicated MEF scheme, but theoretically much more effective, was to use silver nanocubes on the substrate to enhance the fluorescence. In this scheme, the phenomenon could be tested on glass because the refractive index will be what light travels through to hit the cubes. This will not change based on what is below the cubes. Also, SAW device was changed to quartz which is similar in structure to glass.

The cubes were made using a colloidal synthesis from Zhang et al.[33] 30 mL of ethylene glycol (Sigma-Aldrich) was added to a 250-mL round bottom flask and heated under magnetic stirring in an oil bath preset to 150 ^{o}C. After 30 minutes of heating, 0.36 mL of 3 mM NaHS (Sigma-Aldrich) in ethylene glycol was injected into the heated solution. Two minutes later, 3 mL of 3 mM HCl (Sigma-Aldrich) and 7.5 mL of poly(vinyl pyrrolidone) (PVP) (Alfa Aesar), both in ethylene glycol, were injected into the solution. After another 2 minutes, 2.4 mL of 282 mM CF_3COOAg (Sigma-Aldrich) in ethylene glycol was injected into the solution. The flask was capped during the entire synthesis except during the addition of reagents.

Following the addition of the CF_3COOAg solution, vapors formed in the flask and the clear solution took on a yellowish color within 2 minutes. This change in color indicated that the nucleation of Ag seeds had begun. The solution proceeded to shift colors from red, to reddish grey, and finally to a greenish color with red, orange and blue undertones. 50 minutes after the addition of the CF_3COOAg, the flask was transferred to room temperature water to quench the

reaction. The Ag nanocubes were washed with acetone once which was followed by three cycles of washing with ethanol to remove excess PVP via centrifugation. The Ag nanocubes were then dispersed in ethanol for characterization and storage. The LSPR peak positions were analyzed using UV-VIS spectroscopy (PerkinElmer Lambda 35) by recording their extinction spectrum. TEM (Phillips, FEI Morgangi TEM) images were taken to analyze shape and size distributions.

The silver nanoparticle solution that was made should theoretically contain 2.19638×10^{11} cubes per mL of solution. To ensure proper spacing, 50 uL was dropped on the surface. This should result in slightly over one-fourth of the surface to be covered with silver nanocubes. This should give proper spacing while also having enough particles on the surface. This is found with the following calculations. The bottom area of one cube is

$$50\ nm\ x\ 50\ nm = 2{,}500\ nm^2 \tag{25}$$

Meanwhile, one-fourth of the area of the substrate is

$$\frac{1}{4}\ x\ 1\ cm\ x\ 1\ cm = 0.25\ cm^2\ x\ \frac{10{,}000{,}000^2\ nm^2}{1\ cm^2} = 25{,}000{,}000{,}000\ nm^2 \tag{26}$$

This means that the total number of cubes needed is

$$\frac{25{,}000{,}000{,}000\ nm^2}{2{,}500\ nm^2} = 10{,}000{,}000{,}000\ nanocubes \tag{27}$$

In one milliliter of solution, approximately 2.19638×10^{11} nanocubes are made. Therefore, the total amount of solution that must be used is

$$\frac{1x10^{10}}{2.1963x10^{11}}\ x\ 1\ mL\ x\ \frac{1{,}000\ \mu L}{1\ mL} = 45.5\ \mu L \tag{28}$$

Six different concentrations of goat anti-rabbit IgG tagged with Alexa-488 were prepared. Since the antibody is received at 2 mg/mL, two uL were initially pipetted out and mixed with 38 uL of PBS to create a concentration of 100 ug/mL. From this solution, 1 uL was taken and mixed with 9 uL of PBS to create a concentration of 10 ug/mL. This process was continued until

concentrations of 100 ug/mL, 10 ug/mL, 1 ug/mL, 100 ng/mL, 10 ng/mL, and 1 ng/mL were prepared.

Two different sets of glass cover slips, each containing six glass cover slips, were then prepared. Both were silanized with 3-glycidoxypropyldimethylethoxysilane (3-GPDMS) using a procedure from Cular et al.[16] Essentially, a one percent 3-GPDMS solution in toluene covers the surface for 1 hour. The slides are then washed with toluene, dried with nitrogen, and heated at 125 degrees Celcius for 1 hour to complete the silanization.

One set of the slides were coated with the 50 µL of silver solution, while the other had nothing done to it and served as a control. Then, each slide was subjected to 10 µL of solution at one of six concentrations prepared, incubated in a humidity chamber for 20 minutes, pipetted off and rinsed thoroughly three times with 10 µL of PBS, and then imaged with the Leica 4000DMI B microscope. Whenever rinsing is mentioned, pipetting and three times rinsing is the method.

3.5.3 Nanocubes to Detect Antigens

MEF is only useful if it can be used to detect different concentrations of solutions. Therefore, the next experiments were done to detect an antigen. In this case, that antigen was normal rabbit IgG. The normal rabbit IgG was received from Invitrogen at a concentration of 0.5 mg/mL. It was then diluted down to different concentrations with PBS. The range of concentrations was from 1 ng/mL to 100 µg/mL.

The procedure was the same as that performed in section 3.5.2. Control groups were again done and compared to the slides with nanoparticles. Silanization was again done and nanoparticles added to one set of slides. At this point, 10 µL of the different concentrations of normal rabbit IgG were added and incubated for 45 minutes which was followed by a PBS rinse.

To ensure that the primary antibody being attached does not attach to the silane, the rest of the attachment sites must be blocked. In this experiment, Bovine serum albumin (BSA) was used to do the blocking. 10 µL of BSA diluted down to 1 mg/mL with PBS was added and incubated for one hour.

Following this, 10 µL of goat anti-rabbit IgG was added and incubated for 30 minutes. The concentration of this was kept constant at 10 µg/mL. For each concentration, three different sets of experiments were performed.

3.6 MEF Results

Both sputtering and colloidal nanoparticle synthesis proved capable of causing MEF, with nanocubes proving to be more effective. While sputtering was simpler to do, nanoparticles were more effective. Also, the difficulties encountered in attaching antibody to silver were too high for sputtering to be a worthwhile technique. Therefore, this technique was abandoned for detection even though it managed to show substantial MEF.

3.6.1 Sputtering Results

Even though the best AFM results came when the silver was sputtered for 90 seconds onto a lithium niobate chip, the best sputtering time for MEF was 180 seconds followed by 270 seconds. When sputtering was done for 90 seconds, the silver was too thin and was removed quickly when liquid antibody solution was applied. When the chip was sputtered with silver for 180 and 270 seconds, the film became smoother but was no longer removed.

Using ImageJ, the pixel intensity was measured and color-coded. The results for sputtering are shown in Figure 3-4, and the corresponding light intensity values are shown in

Table 3-1. This color-coding was only done for the cases where only MEF is studied. This is to really show the high impact of the MEF.

Figure 3-4. MEF results when sputtering a silver layer. a) is the control group without silver (identical to sputtering 90 seconds), b) was sputtered with silver for 180 seconds, and c) was sputtered with silver for 270 seconds.

Table 3-1. Intensity values from measurements with the Leica 4000DMI B microscope.

Sputtering time	Light intensity (a.u.)
Control	18.3
180 seconds	210.9
270 seconds	115.6

3.6.2 Nanocube Results

MEF was also tested using silver nanoparticles. The size of the particles was determined to be around 50 nm with approximately 2.19638×10^{11} cubes present per mL of solution. Between 70 and 90 percent of the nanoparticles were cubes with pyramids, spheres, and rectangles also present. The cubes ranged in size from mostly 40-60 nm. The absorbance of the cubes was measured using a UV-VIS machine and is shown in Figure 3-5. The peak absorbance was found to be 449 nm. Below, in Figure 3-6, a TEM image of the nanocubes can be seen. Many TEM images were taken and this one is representative of the samples as a whole. As can be seen, uniformity is not great.

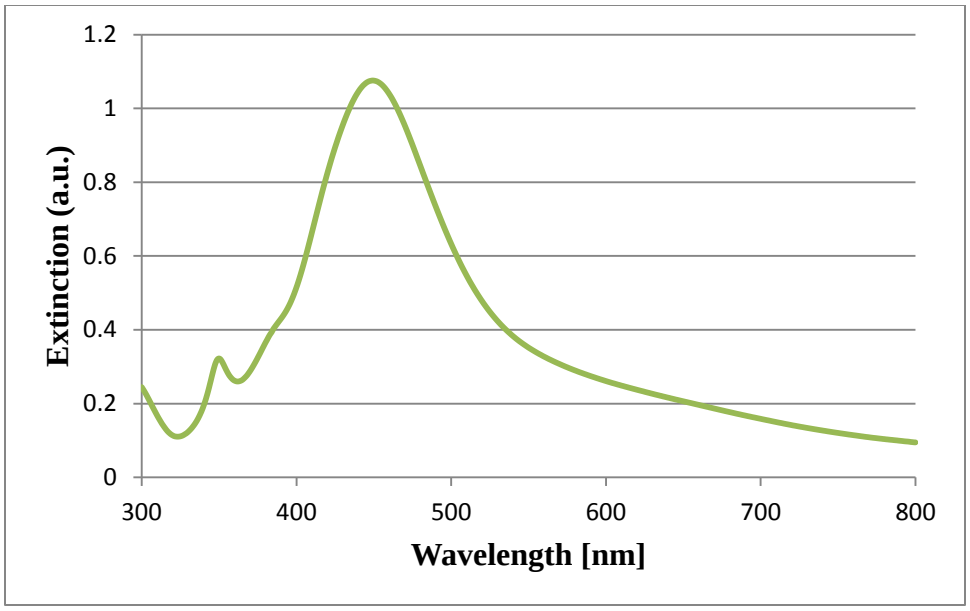

Figure 3-5. Extinction of 50 nm silver cubes in ethanol.

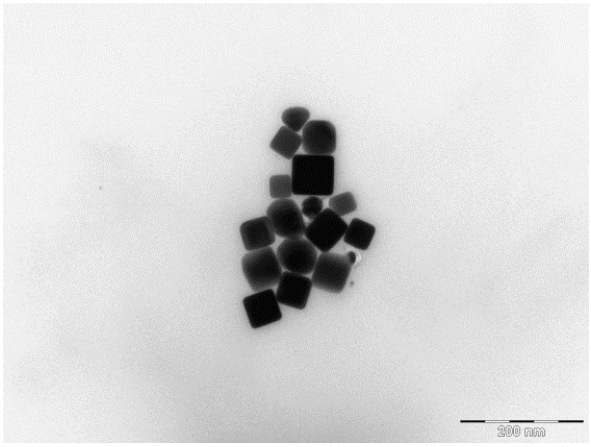

Figure 3-6. TEM image of the nanocubes used in this work.

Even though this extinction does not match up directly with the excitation spectrum of Alexa-488, there is still a large overlap. Once the slides were coated with the nanocubes, six different concentrations were used to measure MEF with and without silver, and the results showed good improvement when silver was used. The images can all be seen in Figure 3-7, and the intensity values can be seen in Table 3-2. The amount of enhancement seen varies somewhat due to the amount of exposure done with the microscope resulting in a wide range.

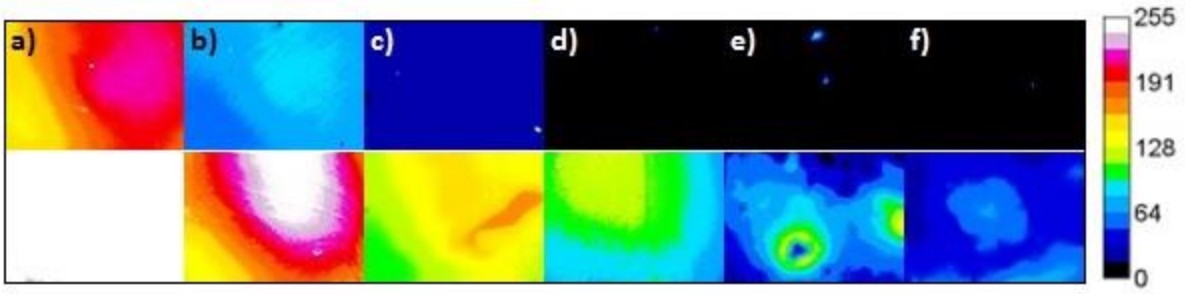

Figure 3-7. Images were taken using the Leica DMI4000 B microscope. The top row shows the control group which had no silver. The bottom row had silver nanocubes with 50 nm dimensions spaced at approximately 150 nm. The concentration of fluorophore used was a) 100 ug/mL, b) 10 ug/mL, c) 1 ug/mL, d) 100 ng/mL, e) 10 ng/mL, and f) 1 ng/mL.

Table 3-2. Light intensity values with and without silver nanocubes. Concentrations range from 1 ng/mL to 100 µg/mL of fluorophore.

Concentration	Intensity without silver	Intensity with Silver
100 µg/mL	186.2	254.7
10 µg/mL	72.4	202.6
1 µg/mL	23.7	134.4
100 ng/mL	7.1	99.0
10 ng/mL	7.7	78.1
1 ng/mL	7.1	43.8

According to many sources the rate of excitation of the fluorophore is proportional to the square of the incident intensity.[2] With the Leica 4000DMI B microscope, the incident intensity was found. With that knowledge, the amount of metal-enhanced fluorescence can be determined by dividing the silver intensity by the control intensity and squaring the result. Also, since the lowest signal the camera can take is 5, this number gets subtracted before analysis.

Table 3-3. Amount of MEF for all the cases mentioned above.

Experiment	Sputtering time (s)		Fluorophore concentration near nanocubes					
Case	180	270	100 ug/mL	10 ug/mL	1 ug/mL	100 ng/mL	10 ng/mL	1 ng/mL
MEF	240.0	69.3	1.9	8.6	47.8	1991.8	742.4	336.5

3.6.3 Detection Results

The last experiments solely concerning MEF were to detect normal rabbit IgG. Three sets of data were achieved for each concentration with more sample point taken closer to 1 ng/mL and fewer above 500 ng/mL. The data show a significant amount of non-specifically bound protein. Also, it shows a significant amount of enhancement for NSBPs when MEF is present. This was proven by doing an experiment with no normal rabbit IgG on the surface.

Besides this, no significant difference can be seen below 400 ng/mL when MEF is not utilized. With MEF, a difference can be seen as low as 1 ng/mL. However, the difference between 1 ng/mL and 10 ng/mL is not high, which could be problematic if extremely accurate results are required. The results can be seen in Figure 3-8.

To test for reproducibility, all of the tests at the different concentration were performed three times each. This allows a standard deviation to be found and error bars are also presented on the graph. A straight line can be seen with MEF and the characteristics of this line are also presented on the graph. At this low concentration, the control does not have a linear shape. A good line for it can be seen at higher concentration in Figure 3-9.

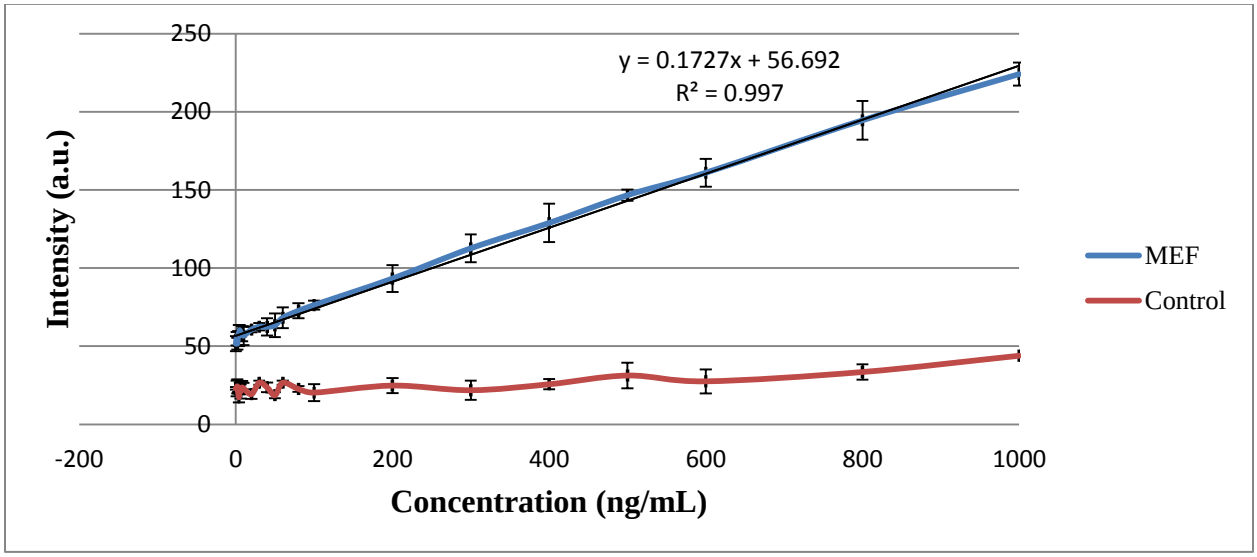

Figure 3-8. Control versus MEF when detecting between 1 and 1000 ng/mL.

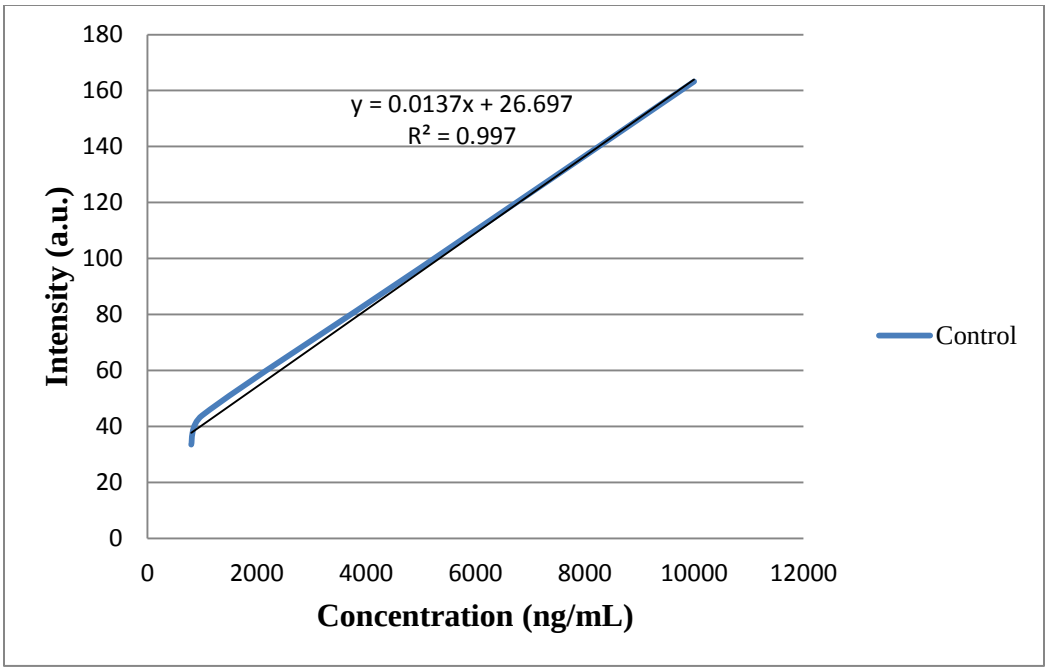

Figure 3-9. Control group between 800 ng/mL and 10,000 ng/mL.

3.7 Discussion on MEF Results

As mentioned above, sputtering is not a great method to cause MEF for detection because it is not as effective as nanoparticles and because it is much more difficult to attach to silver than it is to quartz or silane. Also, sputtering is not consistent and peaks vary wildly from trial to trial. This could be because the CRC sputterer does not keep pressure constant. Higher pressure mostly resulted in more peaks while lower pressure resulted in more flat films. Therefore, nanoparticles were preferred.

As can be seen in Table 3-3, the amount of MEF varies wildly for the nanocubes based on the amount of fluorophore used. One reason for this is that, for the higher concentrations, the camera caps the intensity at 255. If the sample were exposed for a shorter time, the intensity of the control would go down and the sample with the nanocubes should stay the same. In essence, the best way to say put it is that a control group was only able to detect 1 ug/mL while the nanocubes were able to detect at least 1 ng/mL and probably lower. This is a difference of 1000

and that might be the most reliable number to use for the MEF of the nanocubes. For sputtering, not much of the intensity hit 255 for either case and therefore the results of 240 and 69.3 times enhancement are fairly accurate.

Therefore, for detection, silver nanocubes are the best way to proceed because of the greater MEF and the ease with which to attach in the vicinity of the cubes. The enhancement of the cubes is not as high as it could be, however. Future research can focus on fixing the distance between the cubes and the fluorophore as well as a better method for placing the cubes at exact distances from each other.

The problems with the detection using nanocubes are also plentiful but are insignificant enough at this point to where the procedure will still work. As the error bars in Figure 3-7 show, the standard deviation is not small enough to where a difference can be seen from 1 ng/mL to 2 ng/mL. Also, a trial at 10 ng/mL could potentially show an average of 1 ng/mL. This is a significant problem. However, with this method, a difference between 1 ng/mL and 20 ng/mL is easy to see whereas without MEF, a difference cannot be seen from 1 ng/mL and 400 ng/mL. Therefore, this is significant improvement.

The reasons for this are plenty. Most likely, it is due to non-uniform spreading of the particles. For these experiments, the nanoparticle solution was drop-coated. This will results in a higher density of cubes in certain areas. The best way to fix that would be to use an imprint lithography technique which is outlined in a dissertation by Verschuuren.[34] If this method were to be too expensive, another method could be to use spin-coating to evenly distribute the particles.[35] Another potential reason for this deviation is that only 70-90 percent of the shapes are cubes and not all are 50 nm edge lengths. If a higher proportion of something else were to be on the slide, more deviation would occur.

The MEF currently being shown can be improved upon. The extinction peak is only 449 nm here whereas the excitation peak for Alexa-488 is 488 nm. By moving the extinction peak closer to 488, more MEF would occur. Currently, two methods are being researched for doing this. One is to make the refractive index higher. FDTD Solutions simulations show that a higher refractive index will red-shift the peak. This could be done by sputtering SiO_2 onto the surface of the cubes. This would also result in a more stable environment for the cubes. Another method would be to make bigger cubes. As FDTD Solutions simulations show in section 3.4, bigger cubes will also red-shift the peak.

CHAPTER 4: REMOVAL OF NON-SPECIFICALLY BOUND PROTEINS BY SAW

SAW, short for surface acoustic wave, devices have a lot of uses in many different applications, primarily in sensing. It has never been used in conjunction with the immunofluorescence technique, however. The acoustic waves generated by the SAW device can improve the technique in numerous ways.

As mentioned previously, immunofluorescence suffers from background signals, also known as "noise." This can be due to autofluorescence or overlapping spectra of other proteins or fluorophores.[15] Normally, these background signals are accounted for with compensation by a device such a flow cytometer. This is fine if you know exactly how big an effect the "noise" has, but that is usefully impossible to pinpoint perfectly, especially when the problem is not due to multiple sensing. This then inevitably results in some false-positives and false-negatives during disease diagnosis.

Many studies have been performed showing the removal of weakly bound species by the use of the acoustic streaming from the SAW device using lithium niobate as the piezoelectric material. By keeping the power applied to the SAW at an optimal level, the weaker bound species, such as non-specifically bound proteins (NSBPs), can be removed while the specifically bound proteins remain attached.

This chapter will describe the work that has already been done in SAW removal, the different methods required when combining removal with MEF, and the optimal conditions found thus far in which to perform the removal when MEF is involved and when it is not. This

chapter will also discuss a new sensing material through the use of quartz as the piezoelectric material instead of the use of lithium niobate, which has already been shown.[16]

4.1 Fundamentals of SAW Devices

A surface acoustic wave (SAW) is an acoustic, mechanical wave that propagates within the confines of the surface of a cut piezoelectric crystal. An acoustic wave sends Rayleigh waves through the quartz piezoelectric material and longitudinal waves across the surface.[16] This can be seen for quartz in Figure 4-1. When it comes in contact with something on the surface, the wave velocity and/or amplitude can be greatly affected. The fundamental mode is what is used for removal and micro-mixing.

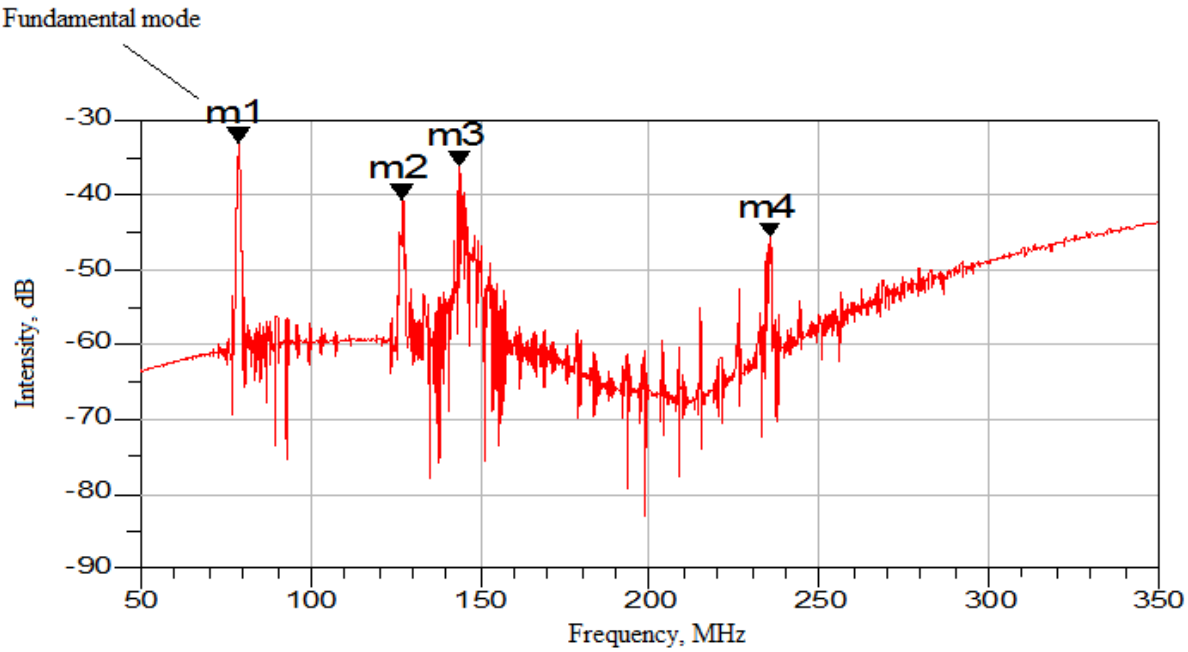

Figure 4-1. Waveform of SAW device with quartz substrate.

Typically, the SAW device is made up of the piezoelectric substrate, the input and output interdigital transducers (IDTs), and the guiding layer between the two IDTs. The input IDT

converts an electrical signal into polarized transversal waves which can travel parallel to the sensor surface along the guiding layer. The output IDT allows for all the acoustic energy to stay concentrated instead of propagating over the entire piezoelectric surface, and then it takes the wave and converts it back into an electrical signal. SAW sensors are sensitive to changes in mass, density, viscosity, and acoustic coupling. A common diagram depicting the SAW device is shown in Figure 4-2.

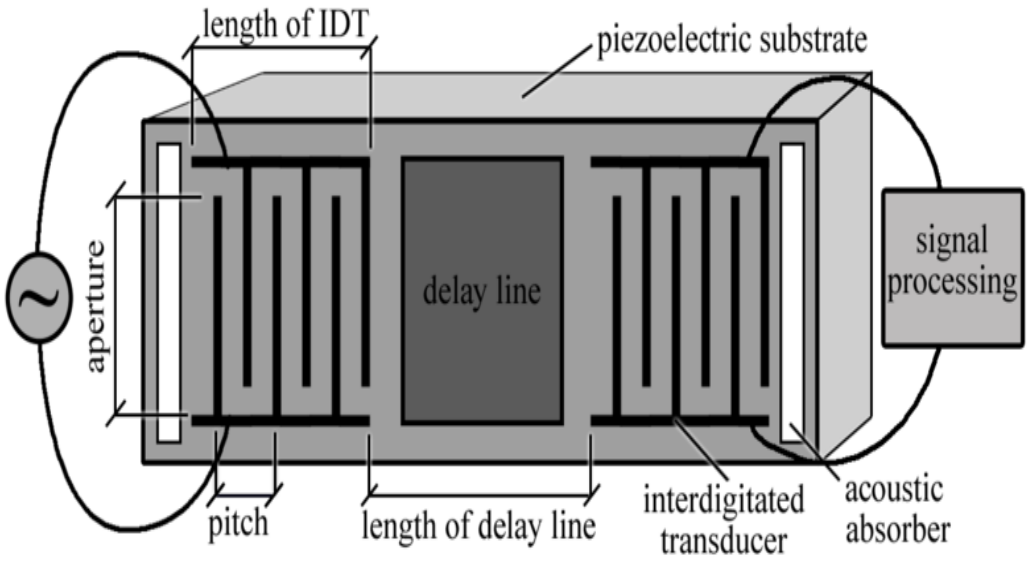

Figure 4-2. Diagram of a typical SAW device.[36]

4.2 Removal Work in Literature

Immunofluorescence techniques commonly suffer from background signals that diminish the effectiveness of the signals desired. Background typically can include other fluorophores that have some overlap with the fluorophore being used, or it can be biofouling, which can be something as simple as dust or other particles that cause some reflection that interferes with the signal. If testing for a cancer biomarker such as AFP or Bcl-2, the signal could come back stronger or weaker than it actually is, potentially leading to a false prognosis. This would ruin the

entire purpose of using the immunofluorescence technique to determine concentration to begin with.

Many different quantification methods are used to try and remove the background. For instance, if using a spectrofluorometer, an option is to measure the signal without your fluorophore, then measure the signal using your fluorophore, and subtract the first data from the second data. This not only adds more work, but it assumes that all the fluorophore added by the user will attach specifically. This is not the case.

To account for this, another trial without specific attachment is required to test how much of your antibody is specifically bound. This again adds more time and more resources to the experiment. It also is not perfect because a surface without any specific binding molecules will have more room for non-specific attachment. That small error could be the difference between a positive and a negative prognosis of cancer.

After all is said and done, the best-case scenario is one in which the background fluorescence is not there at all. Fortunately, studies have shown the ability of SAW devices to remove some of this background. Cular et al. did numerous studies on removal from a lithium niobate surface. In their work, removal of biofouling was shown as was removal of non-specifically bound proteins.[16]

Strong attachment by the specific proteins is of the utmost important, and is the reason that a sputtered film of silver will not be as effective as using nanocubes. By using nanocubes, a similar method of attachment with silane can be used for the device around the nanocubes. Sputtered silver would require direct attachment of the antigen/antibody to the silver. This is not easy to do because silver is not reactive.

4.3 Experimental Procedure

In this part of the research, MEF was not yet added to the work. First, showing non-specific binding was shown. This was done in numerous different ways. A spectrofluorometer was used to show the binding of components in urine and other sensing marker. It was also shown using the Leica DMI4000 B microscope. Then, removal of the non-specific binding with SAW waves was performed.

4.3.1 Procedure for Showing Non-Specific Attachment

Initially, the effect of non-specific attachment on sensing had to be shown. Using a PC1 spectrofluorometer from ISS, the emission from three different samples being excited at 488 nm was measured. The first sample was 1 µg of donkey anti-mouse tagged with Alexa-488 in PBS. The second sample still had the 1 µg of donkey anti-mouse tagged with Alexa-488 but also had 1 µg of goat anti-mouse tagged with Alexa-546. The third sample was the same as the second sample but with 2 µg of goat anti-mouse tagged with Alexa-546. The results from this can be seen in the Results section in Figure 4-3.

Another method of showing non-specific attachment was done using the Leica DMI4000 B fluorescence microscope. Here, 10 µL of BSA was added to a glass slide at a concentration of 1 mg/mL and incubated for 1 hour. Then, 10 µL of goat anti-rabbit antibody tagged with Alexa-488 was added at a concentration of 10 µg/mL for 30 minutes. This was rinsed three times with 10 µL of PBS before imaging. Again, the results can be seen in the Results section and specifically Figure 4-4.

Finally, different proteins and organic acids which are present in different concentrations in urine were measured using the PC1 spectrofluorometer.[37] Again, the fluorophore by itself was

measured and this was followed by the addition of the proteins and organic acids. These results can be seen in Figure 4-5.

4.3.2 Procedure for Showing Removal

To show removal, a quartz SAW device was patterned with AZ 4620 (AZ electronic materials) photoresist leaving squares with 20 µm sides spaced 20 µm apart not coated with photoresist. Then, following a method from Cular et al., the SAW device was silanized with 3-GPDMS following the method mentioned in Chapter 3.[16] This was followed by a thorough acetone rinse to remove the photoresist. This leaves the 20 µm squares with silane while removing the silane that is attached to the photoresist. Therefore, you end up with specific attachment inside the squares and non-specific attachment outside of the squares.

To keep the fluid area constant, an O-ring was placed on the guiding layer between the input and output IDTs of the SAW device. Then, 10 µL of rabbit IgG at a concentration of 100 µg/mL was pipetted onto the area inside the O-ring and incubated in a humidity chamber for 45 minutes. This was followed by a PBS rinse identical to that used above. Then, BSA was added for 1 hour in the same way it was for the non-specific binding experiment above. Finally, 10 µL of goat anti-rabbit IgG tagged with Alexa-488 was added at a concentration of 10 µg/mL and incubated for 30 minutes. After this time, rinsing was performed again and imaging done. Then, SAW power at 10 mW was done for 5 minutes and imaging done again.

After this removal was completed, non-specific donkey anti-mouse tagged with Alexa-488 was added to the SAW device and rinsing and removal were done again, also at 10 mW, with images after each step. Finally, an amplifier was used to increase the power of removal for another 5 minutes and one final imaging step performed.

4.4 Removal Results

Figure 4-3 shows the effect of adding Alexa-546 to a solution with Alexa-488. As more Alexa-546 is added, the intensity of the Alexa-488 decreases. The peak at 523 nm, which corresponds to Alexa-488, is decreasing, and the intensity above 560 nm, which corresponds to the lower emission lengths of Alexa-546, is increasing slightly. This is due to the lower part of the excitation spectrum of Alexa-546 emitting at the higher emission wavelength of Alexa-546.

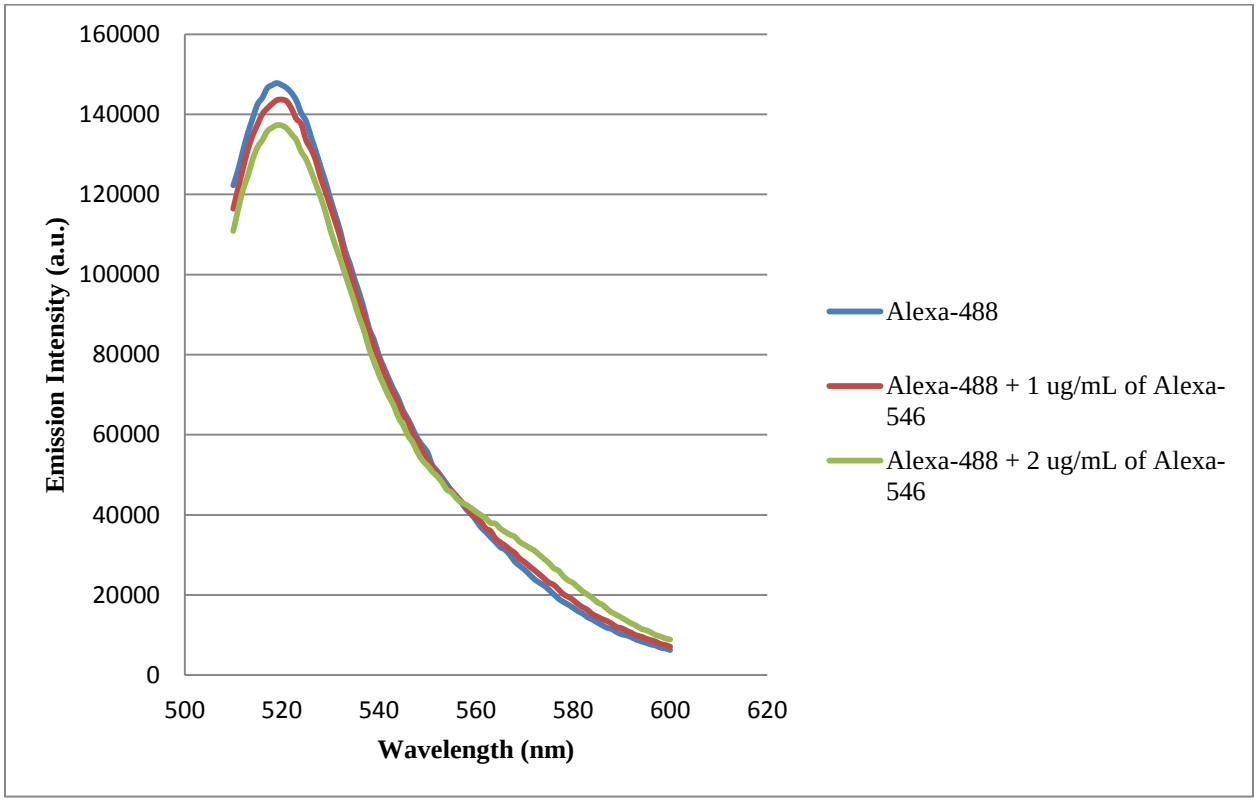

Figure 4-3. Effect of multiple sensing on the emission of Alexa-488

Figure 4-4 shows the effect of non-specific binding. As can be seen, there is a lot of non-specific binding when removal is not being used. While the BSA is able to block successfully in certain regions, it does not manage to cover the whole surface even though the amount added should be more than capable of saturating the surface.

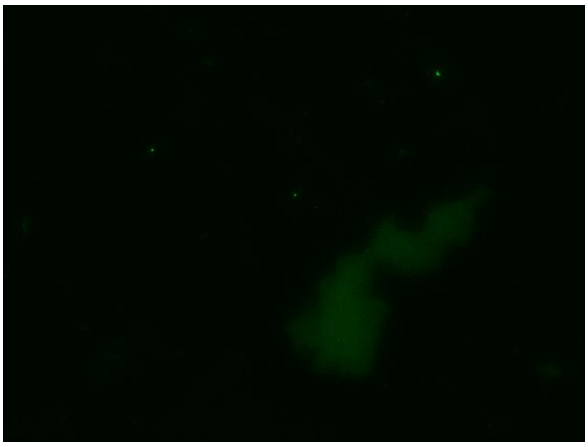

Figure 4-4. Non-specific attachment which can easily skew the data.

The last experiment to show non-specific attachment was with different substances known to be present in urine, which is something that could be used to test for biomarker concentrations. Some of the substances were organic acids such as oxalic acid, acetic acid, and benzoic acid. For good measure, the protein BSA was also included, and it was the last compound added.

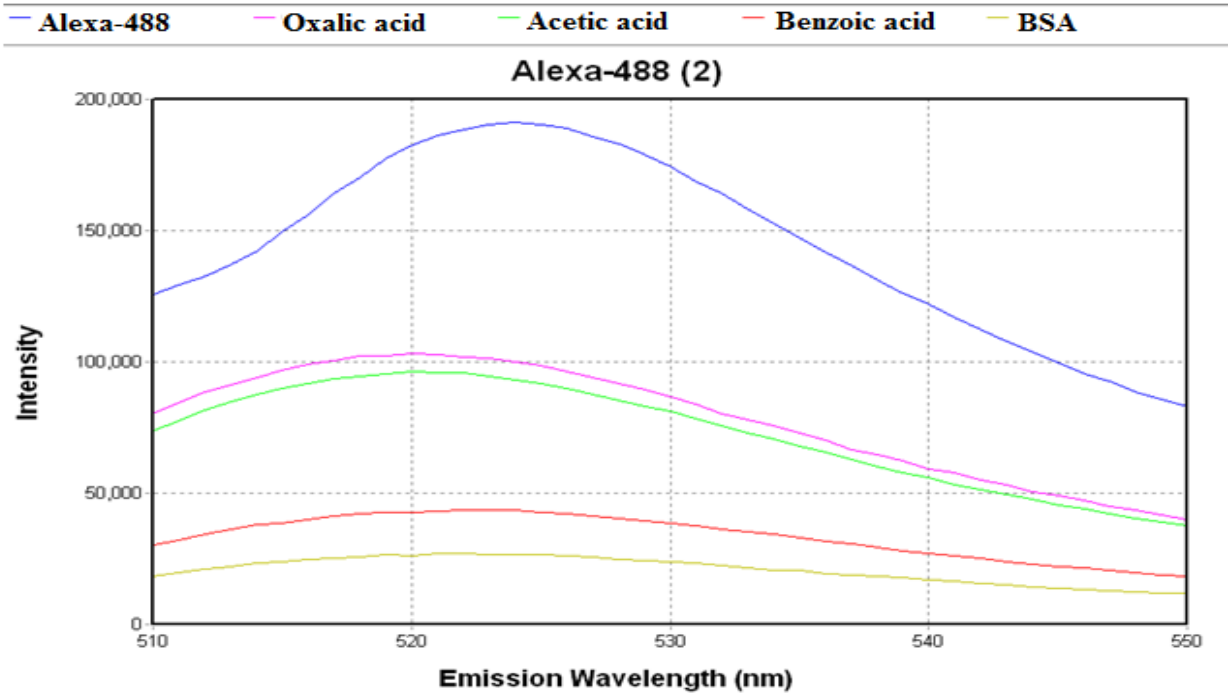

Figure 4-5. Effect of components in urine on the emission intensity of Alexa-488.

The first removal experiment done was with specific attachment. Then non-specific attachment was done and finally power amplification was done and imaging done close to the input IDT and at the center. The before and after removal images for specific and non-specific attachment are shown in Figure 4-6. Images after power amplification are shown in Figure 4-7 and intensity values for all cases at 10 mW are in Table 4-1 while intensity values for increased power is in Table 4-2.

In Figure 4-6, parts a) and b) are the important aspects for the current usage of the MEF-SAW device. Parts c) and d) become important when multiple sensing is done and another antigen is being tested for at the same time.

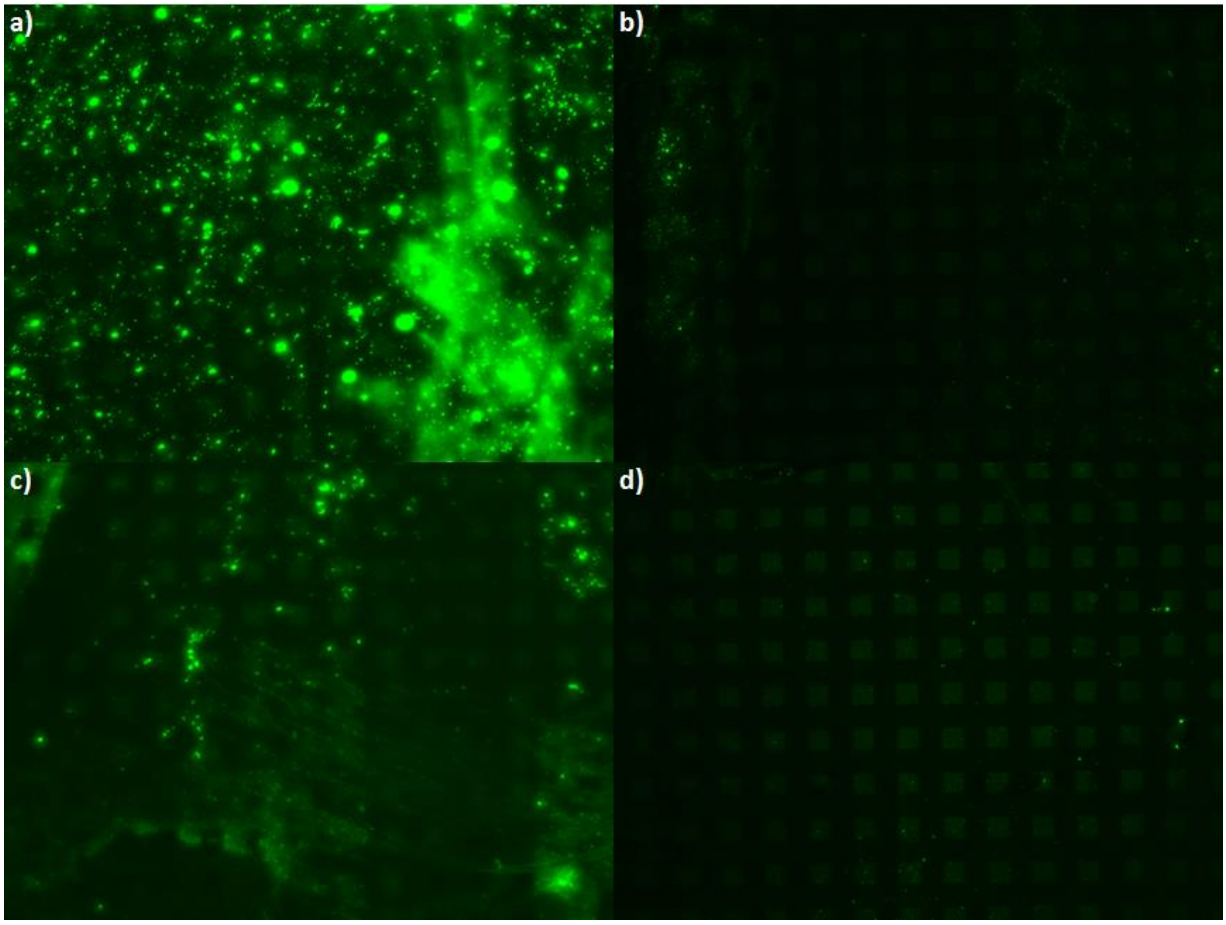

Figure 4-6. Results for removal. a) shows goat anti-rabbit binding after rinsing but before removal, b) shows goat anti-rabbit binding after removal, c) shows donkey anti-mouse binding after rinsing but before removal, and d) shows donkey anti-mouse binding after removal.

Table 4-1. Intensity values for images in Figure 4-6.

Case	Before removal	After removal
Goat anti-rabbit in squares	120.3	20.1
Goat anti-rabbit outside squares	93.9	12.9
Donkey anti-mouse in squares	47.4	31.0
Donkey anti-mouse outside squares	37.5	16.1

The information from Figure 4-7 will be more important when recycling of SAW devices will become desired. For now, that is not something being studied extensively.

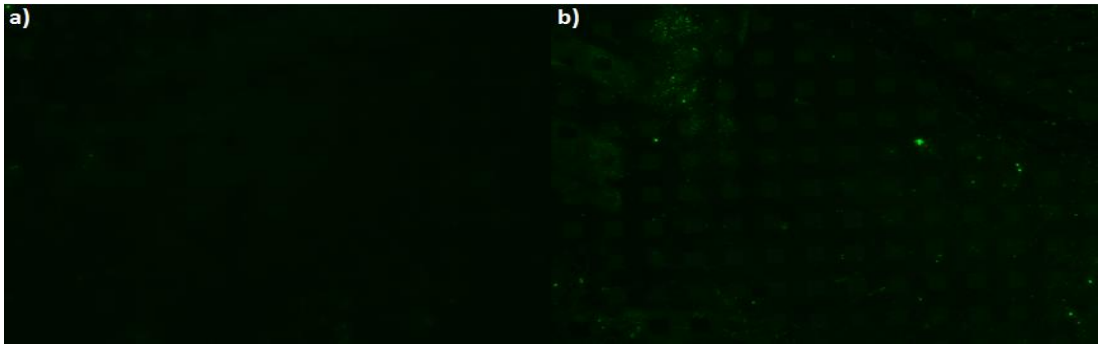

Figure 4-7. Removal after power amplification. a) shows the amount of removal near the input IDT while b) shows the removal at the center of the SAW device.

Table 4-2. Intensity values for images in Figure 4-7.

Location	Inside squares	Outside squares
Near Input IDT	15.6	13.1
Center	19.2	14.8

4.5 Discussion of Removal Results

The removal experiments show a number of interesting things. Firstly, the removal here was done with quartz. This is the first time quartz has been shown to be capable of doing removal. $LiNbO_3$ is thought to be better due to a higher electromechanical coupling coefficient. Clearly, Figures 4-6 and 4-7 show removal is being done. Now, the question is how much of it is specific binding and how much of it non-specific binding.

Table 4-1 shows that there are huge decreases inside and outside of the squares for both cases. Of course, just because it is attached inside the square does not mean that the attachment is necessarily specific. There could be regions to attach to non-specifically much like what happens in Figure 4-4. What is clear is that the regions outside of the squares is all non-specific binding and this decreases slightly less than the squares when using specific goat anti-rabbit IgG and slightly more when using non-specific donkey anti-mouse IgG. This does indicate that some specific attachment is being removed, but not as much as the non-specific binding being removed.

The fact that there is an increase inside the squares after attaching donkey anti-mouse after removal indicates that there is some more non-specific attachment inside the squares that has not completely been removed. However, the intensity difference is only 3.2 which is nearly zero based on these types of intensity readings.

What these results indicate is that removal is being done; however, these results also indicate that a better mechanism for primary attachment than the use of an epoxy silane is needed. In these experiments, an epoxy silane was used because it worked for Cular et al. Most sources indicate that other silanes would be more useful such as an amino silane. Wong and Burgess mention that 3-aminopropyl trimethoxy silane (APS) is widely used to attach silica to antibodies. However, they also mention that to get stronger covalent bonds, better materials such as N-5-azido-2-nitrobenzoyoloxysuccinimide (ANB-NOS) is even better.[38] To get better removal of only non-specific binding, a stronger attachment is needed. To get complete removal of non-specific binding, the power input needs to be increased to the point where it removes more while not frying the antibodies.

CHAPTER 5: INCREASED MIXING FROM ACOUSTIC STREAMING BY SAW

Improving the testing time of immunofluorescence assays can be an important aspect to improve. Of course, the most important thing is to get clean and accurate detection, which is achieved through MEF and removal of NSBPs. After this is achieved, however, the focus can be placed on secondary aspects such as making the procedure quicker to perform. More work can be accomplished if a procedure takes 30 minutes versus two hours with fewer resources getting needlessly wasted. In some cases, attachment is so complicated that even days can be required, and it is especially in these situations that micro-mixing can be so important.

5.1 Previous Work on Micro-Mixing

Increased mixing of a substance due to the acoustic streaming of a SAW device has already been shown to different degrees. It has not, however, been experimentally shown to increase the attachment of antibody to antigen in the immunofluorescence assay technique. The theory is that the acoustic streaming causes the secondary antibody to float around quicker increasing the likelihood that it will find a binding site more quickly. Essentially, this works to remove mass-transport-limited diffusion. Another way to look at it is as a reverse removal scheme. Instead of removing loosely-bound material, it causes the specifically attached material to find attachment spots more quickly. Also, rinsing is a big part of removal, and that is not a key aspect in mixing.

In 2008, Paxton et al. used single-bead anion exchanges of plutonium to successfully demonstrate acoustic mixing. Using an uptake reaction, they then measured the remaining plutonium after a certain amount of time when acoustic streaming was used and when it was not used. They managed to find uptake with acoustic streaming that happened 5.8 times faster than when static diffusion was used.[19] To show how significant this is, an immunofluorescence technique that takes two hours could be finished in about 20 minutes. Even more significantly, a procedure that takes two days could be done in a little over 8 hours.

5.2 Experimental Procedure to Show Micro-Mixing

The testing for increased mixing was done in a similar method to the removal experiments. Again, 10 µL of normal rabbit IgG was incubated for 45 minutes inside an O-ring in the middle of the SAW device. Then, PBS rinsing was done followed by BSA blocking (1 mg/mL) for 1 hr. This was done for all the different experiments. In final practice, the thought is that these steps can also be improved with micro-mixing. For this thesis, only improving the secondary attachment was considered.

After these steps, control experiments were first done. Secondary goat anti-rabbit IgG tagged with Alexa-488 at a concentration of 10 µg/mL was incubated from between one minute to one hour to see how long saturation takes. This was then followed by PBS rinsing and imaging with the Leica DMIb 4000 microscope to get fluorescence intensity values.

After getting baseline values, the 10 µg/mL of secondary antibody was again incubated but now 10 mW of power was applied for five minutes and followed by rinsing. This was also done for ten minutes. Finally, imaging was again done with the Leica DMIb 4000 microscope.

5.3 Micro-Mixing Results

First, baseline values without using SAW power were found. These studies found that the attachment of goat anti-rabbit IgG to normal rabbit IgG takes approximately 30 minutes. After 20 minutes, the intensity begins to even out, and it does not increase after from incubating between 30 minutes and 1 hour. The results of this study are shown in Figure 5-1.

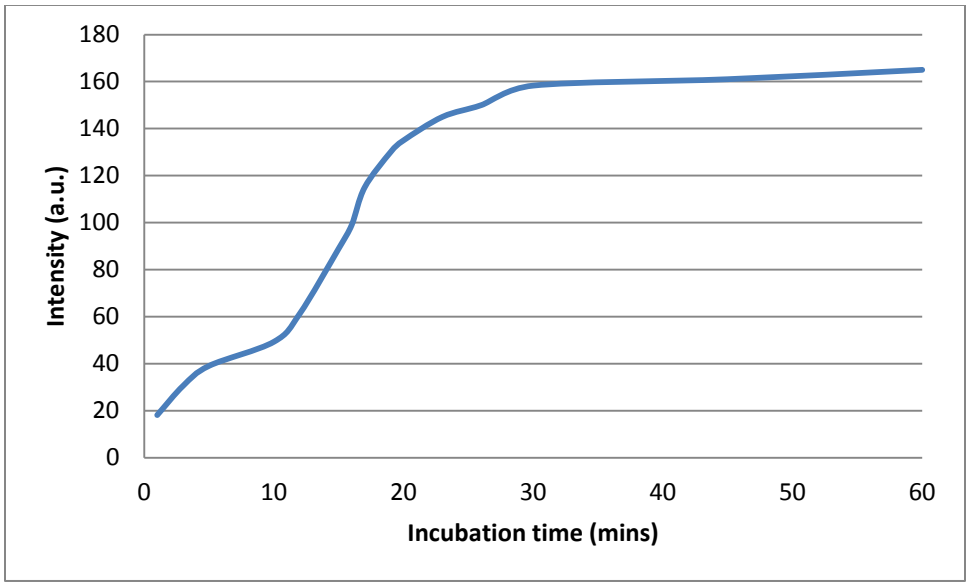

Figure 5-1. Incubation control times. Incubation time to attach secondary goat anti-rabbit IgG to normal rabbit IgG without SAW power.

Only two time experiments were done using the SAW, so this still needs to be optimized. However, the result does show that micro mixing is a possibility. Figure 5-2 shows the difference between five and ten minutes with SAW and without SAW, and Figure 5-3 shows the numerical difference.

As can be seen, five minutes is not enough to reach saturation as it reaches approximately half. Ten minutes, however, does reach the same value as an hour without saturation The control group is nearly saturated after 30 minutes as it reaches 97% of the intensity value after an hour. Fewer attachment spots are available and therefore the line straightens.

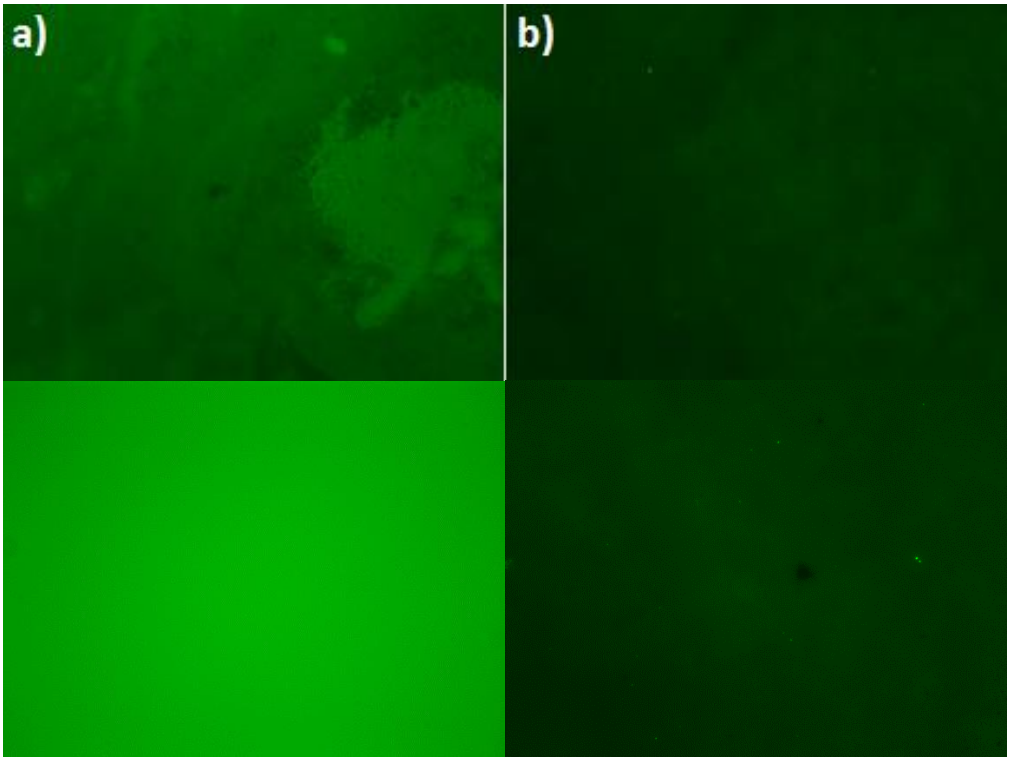

Figure 5-2. Effect of micro-mixing. The amount of attachment a) with SAW and b) without SAW. The top row is for five minutes and bottom is for ten minutes.

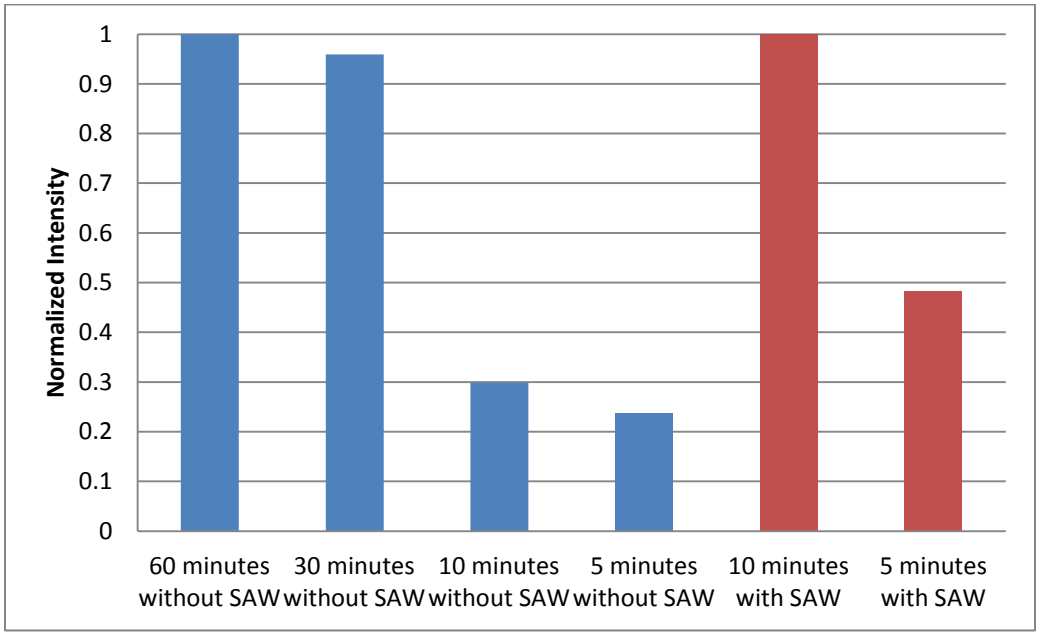

Figure 5-3. Comparing the use of SAW to not using SAW. While 5 minutes with the SAW is better than 10 minutes without the SAW, it is not good enough to saturate the sample. Ten minutes with the SAW is good enough, however.

5.4 Discussion of Micro-Mixing Results

Micro-mixing of fluids with a SAW device is possible and is proven with experimental results. How effective it can be still needs to be optimized. In this work, the difference between fluorophore attachment after five and ten minutes with and without SAW is obvious and is illustrated in Figure 5-2.

For this particular antibody-antigen attachment, it was found that approximately one hour is required for saturation (the point where all available antigen attachment sites have been attached to by antibody). This does not seem like a long time in the overall scheme of things. However, for an IF assay, there are multiple attachments that need to happen. In the particular assay being studied in this work, the antigen (normal rabbit IgG in this case) needs to attach to the surface before anything else can be done. Without SAW, it was found that an optimal time for this would be 45 minutes.

Then, a blocking agent needs to be added. In this case, fetal bovine serum albumin (BSA) was used and an optimal attachment time for that is another hour. This is then followed by the antibody attachment which was found to saturate after 1 hr.

If each of these steps could be cut to five minutes or less, a procedure previously taking almost 2.5 hours could be cut to 15 minutes or less. Again, that is only the potential. In the work done so far, 10 minutes with SAW was able to saturate. This represents an increased diffusion rate of 6. With this increased rate, the traditional method would be 165 minutes and the improved SAW method would only be 27.5 minutes, which is a big improvement.

For this particular attachment scheme, 137.5 minutes is saved. In some eyes, that may not be worth doing everything on a SAW device. However, some attachments take much longer, even requiring days in some cases. Some attachments are so slow that they require overnight

storage. For some of these cases, complete saturation of all the steps could take 24-48 hours. With the increased attachment rate, this could become 4-8 hours, which is a significant improvement and well worth doing the assay on a SAW chip.

Again, the mixing aspect of this experiment still needs to be optimized. Different optimizations could include changing the SAW structure, increasing the power to the SAW without frying the sample, inserting power from both ends of the SAW, and numerous other ideas to really concentrate the acoustic energy in the area requiring micro-mixing.

CHAPTER 6: FINAL DEVICE

Showing that MEF, removal, and micro-mixing are all possible does not prove that the MEF-SAW is possible with this scheme. It needs to be ascertained that the nanocubes are bound tightly enough to the surface so that the acoustic energy does not remove them as well as the NSBPs. If they are not, a new method would be required to secure the nanoparticles more firmly while not affecting the MEF being found with the current technique.

On top of that, it also needs to be ensured that the presence of the nanoparticles does not affect the capability of the SAW to remove the NSBPs and to cause micro-mixing. Therefore, the final experiment required to prove the importance of the MEF-SAW is the combination of all three into an actual immunofluorescence assay.

6.1 Experimental Procedure for the Final Device

Immunofluorescence assays using the MEF-SAW technique is much more complicated than traditional IF, but it makes up for this by being more accurate, having lower detection limits, and being quicker to do.

First, the quartz SAW devices were manufactured in the same method described in Chapter 4. Then, silver nanocubes with approximately 50 nm edge lengths were synthesized colloidally following the method outlined in Chapter 3. Next, an O-ring was placed in the center of the SAW device and 50 μL of the silver nanocube solution was placed inside the O-ring and allowed to dry for 30 minutes at 50 degrees Celsius. This results in optimal spacing for MEF.

To perform the immunofluorescence experiment, 10 µL of normal rabbit IgG with a concentrations of 50 ng/ml was again used as the protein of interest. Based on the micro-mixing rate found in Chapter 5 and the fact that normal rabbit IgG normally requires 45 minutes of incubation, SAW power was applied at 10 mW for 7.5 minutes. This was then followed by a thorough PBS rinse using the same rinsing technique used for all of the other experiments performed.

Following the rinse, 10 µL of BSA with a concentration of 1 mg/mL was used to block. With the knowledge that this usually requires 1 hour to incubate, it was micro-mixed for 10 minutes with 10 mW of power. Again, this was followed by the PBS rinse.

Finally, the detection was again done with goat anti-rabbit IgG tagged with Alexa-488. This concentration is constant at 10 µg/mL and a total of 10 µL was used. Knowing that 1 hour is typically required to fully incubate, a power of 10 mW was applied for 10 minutes to cause the micro-mixing phenomenon. To finish, rinsing was again performed with PBS and then imaging was done with the Leica 4000DMI B microscope using the same parameters as mentioned previously.

After imaging, removal was performed for 5 minutes at 10 mW of power and imaging was done again.

6.2 Final Results and Accuracy

It was to be expected that a similar intensity to that of the graph of in Figure 3-7 at a value of 50 ng/mL would be found after mixing but before removal. This was the case as the intensity without the SAW was around 62.3 and with micro-mixing it was around 64.5. This difference was within the standard deviation. Also, since the no SAW experiment only incubated

the final antibody for 30 minutes (97% of saturation), it should be expected to be slightly lower than when the SAW was used.

After removal, the intensity was expected to be lowered slightly since most of the sample should be specifically bound with a small amount of NSBPs. Again, this was the case as the intensity dropped to 57.6. The corresponding image for this can be seen in Figure 6-1. The images look fairly similar, but the difference is significant.

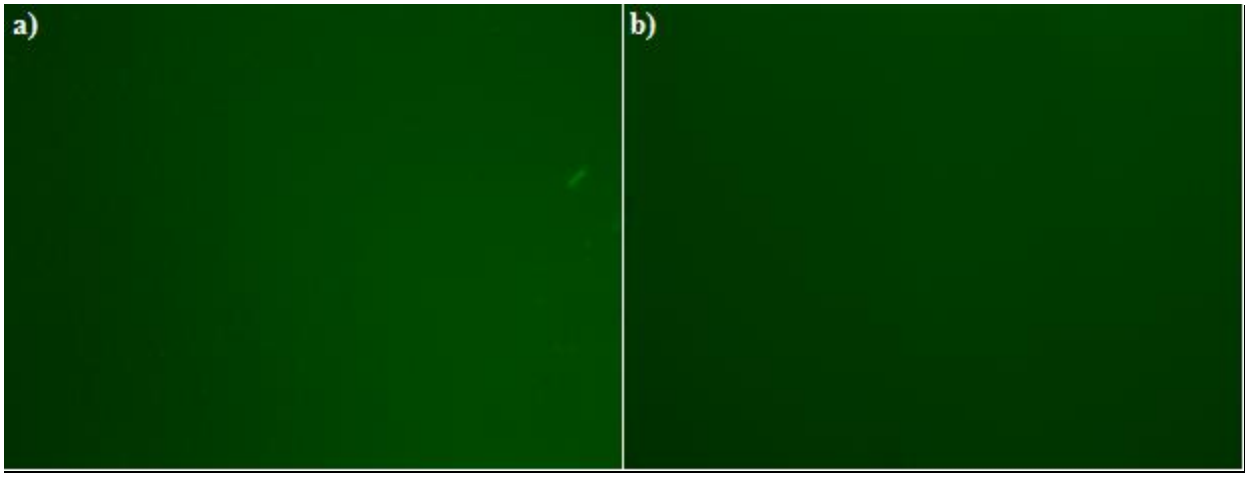

Figure 6-1. Intensity values for the full device. a) was before removal and b) was after removal.

6.3 Discussion on the Total MEF-SAW Device

The final device results show that the device does work but still needs to be optimized. Without any primary antibody, it was shown that the intensity was 52 a.u. when using MEF, which should all be non-specifically bound. Between 5 and 7 a.u. can be seen when no fluorophore is used. Therefore, about 45-47 a.u. needs to be removed when using this exposure time and all other settings used for this experiment. However, only 6.9 a.u. were removed. This is better than removing none but still is not ideal.

Micro-mixing was shown to be effective at 10 mW of power to speed up the diffusion rate six-fold. Considering that few experiments were performed and higher power can be

supplied without frying the sample, better micro-mixing should definitely be possible. A rate of six has been shown in other cases but could potentially be improved on greatly. That is an area that will be focused on in future research.

The next steps in this work will be to improve the removal aspect of the work. That is a critical area and needs improvement. Perhaps it will be found that quartz is not good enough to complete the work and lithium niobate may be required. More testing will need to be done.

After improving removal, the work will focus on testing an actual biomarker. In our case, testing Bcl-2 concentrations in urine will be desired. This is a biomarker that Anderson et al. showed can be a predictor of ovarian cancer. In their work, they found that a healthy individual would have around 0.59 ng/mL, an individual with benign ovarian cancer would have 1.12 ng/mL, an individual with 2.60 ng/mL would have early stage ovarian cancer, and an individual with 3.58 ng/mL would have late-stage ovarian cancer.[39]

In our work, detecting below 1 ng/mL was not done. However, by raising the exposure time or improving the MEF by some of the techniques mentioned, this should be possible. In that case, a control graph could be made for MEF such as the one made in Figure 3-7 and new samples should be able to be measured to determine concentration.

REFERENCES

1. Owen, Judy, Jenni Pent, and Sharon Stranford. *Kuby Immunology*. New York: W.H. Freeman & Co., 2012. Print.

2. Aslan, Kadir et al. "Metal-enhanced fluorescence: an emerging tool in biotechnology." *Elsevier Science Direct,* Current Opinion in Biotechnology, 16 (2005): 55-62. Web.

3. Chowdhury, Sanchari, Venkat R. Bhethanabotla, and Rajan Sen. "Silver-copper alloy nanoparticles for metal enhanced luminescence." *Applied Physics Letters* 95 (2009): 131115. Web.

4. Chowdhury, Sanchari, Venkat R. Bhethanabotla, and Rajan Sen. "Effect of Ag-Cu Alloy Nanoparticle Composition on Luminescence Enhancement/Quenching." *Journal of Physical Chemistry* (2009): 13016-13022. Web.

5. Deng, Wei et al. "Metal-enhanced fluorescence in the life science: here, now and beyond." *Physical Chemistry Chemical Physics* (2013): 15695-15708. Web.

6. Dragan, Anatoliy I. and Chris D. Geddes. "Metal-enhanced fluorescence: The role of quantum yield, Q_0, in enhanced fluorescence." *Applied Physics Letters* (2012): 093115-1-4. Web.

7. Golberg, Karina et al. "Mixed-metal substrates for applications in metal-enhanced fluorescence." *Journal of Materials Chemistry*, 21 (2011): 6179-6185. Web.

8. Gryczynski, Ignacy et al. "Multiphoton Excitation of Fluorescence near Metallic Particles: Enhanced and Localized Excitation." *Journal of Physical Chemistry B*, 106 (2002): 2191-2195. Web.

9. Kowalska, Dorota et al. “Metal-Enhanced Fluorescence of Chlorophylls in Light-Harvesting Complexes Coupled to Silver Nanowires.” *The Scientific World Journal* (2013): 1-12. Web.

10. Lakowicz, Joseph R. et al. “2. Effects of Silver Island Films on Fluorescence Intensity, Lifetimes, and Resonance Energy Transfer.” *Analytical Biochemistry* 301 (2002): 261-277. Web.

11. Morton, Seth, Daniel Silverstein, and Lasse Jensen. “Theoretical Studies of Plasmonics using Electronic Structure Methods.” *Chemical Reviews,* American Chemical Society 111 (2011): 3962-3994. Web.

12. Rycenga, Matthew et al. “Controlling the Synthesis and Assembly of Silver Nanostructures for Plasmonic Applications.” *Chemical Reviews,* American Chemical Society 111 (2011): 3669-3712. Web.

13. Zhang, Yongxia et al. “Metal-Enhanced Fluorescence from Silver—SiO2—Silver Nanoburger Structures.” *Langmuir,* American Chemical Society 26(14) (2010): 12371-76. Web.

14. Odell, Ian D. and Deborah Cook. “Immunofluorescence Techniques.” *Journal of Investigative Dermatology* (2013): 1-4. Web.

15. Robinson, Paul et al. “Immunofluorescence.” *Immunohistochemical Staining Methods*. Fifth Edition. Ed. George Kumar and Lars Rudbeck. Carpinteria: Dako, 2009. 61-65. Print.

16. Cular, Stefan et al. “Removal of Nonspecifically Bound Proteins on Microarrays Using Surface Acoustic Waves.” *IEEE Sensors Journal,* Vol. 8, No. 3 (2008): 314-320. Web.

17. Meyer, Grant D. et al. “Nonspecific Binding Removal From Protein Microarrays Using Thickness Shear Mode Resonators.” *IEEE Sensors Journal*, Vol. 6, No. 2 (2006): 254-261. Web.

18. Miyamoto, Koji et al. “Nonlinear Vibration of Liquid Droplet by Surface Acoustic Wave Excitation.” *Japanese Journal of Applied Physics*, Vol. 41 (2002): 3465-3468. Web.

19. Paxton, Walter F. et al. “Accelerated Analyte Uptake on Single Beads in Microliter-Scale Batch Separations Using Acoustic Streaming: Plutonium Uptake by Anion Exchange for Analysis by Mass Spectrometry.” *Analytical Chemistry*, 80 (2008): 4070-4077. Web.

20. Bakhtari, Kaveh et al. “Experimental and numerical investigation of nanoparticle removal using acoustic streaming and the effect of time.” *Center for High-Rate Nanomanufacturing Publications*. Paper 13. Web.

21. Hayworth, Douglas. “Chemistry of Protein Assays.” *Pierce Protein Biology Products*. Thermo Scientific. Accessed 11 Nov. 2013. http://www.piercenet.com/method/chemistry-protein-assays.

22. Kimball, John W. “Radioimmunoassay.” *Kimball’s Biology Pages*. The Saylor Foundation, 9 Mar. 2011. Web. 12 Aug. 2013. http://users.rcn.com/jkimball.ma.ultranet/BiologyPages/R/Radioimmunoassay.html.

23. *Radioimmunoassays*. Perkin Elmer. Web. Accessed Dec. 12, 2013. http://www.perkinelmer.com/Resources/TechnicalResources/ApplicationSupportKnowledgebase/radiometric/radioimmunoassay.xhtml.

24. “Overview of ELISA.” *Thermo Scientific*. Thermo Fisher Scientific Inc. Web. 12 Aug. 2013. http://www.piercenet.com/browse.cfm?fldID=F88ADEC9-1B43-4585-922E-836FE09D8403.

25. *Abnova Newsletter*. Abnova. Web. Accessed Dec. 14, 2013. http://www.abnova.com/newspaper/1001213/index.html.

26. "Western Blot Procedure." *Davidson Biology Department*. Davidson U, 2001. Web. Aug. 2013. http://www.bio.davidson.edu/Courses/genomics/method/Westernblot.html.

27. *Western Blotting*. The University of Queensland. Web. Accessed Jan. 12, 2014. http://www.di.uq.edu.au/sparqwesternblot.

28. "Immunoprecipitation (IP) technical guide and protocols." *TECH TIP #64*. Thermo Scientific. 2009. Web. Aug. 2013. http://www.piercenet.com/files/TR0064-Immunoprecipitation-guide.pdf.

29. *BD Accuri C6*. BD Biosciences. Accessed Jan. 15, 2014. http://www.bdbiosciences.com/instruments/accuri/.

30. Garoff, Stephen et al. "Electrodynamics at rough metal surfaces: Photochemistry and luminescence of adsorbates near metal-island films." *The Journal of Chemical Physics*, AIP 81 (1984): 5189-5200. Web.

31. Odom, Teri, and George Schatz. "Introduction to Plasmonics." *Chemical Reviews*, American Chemical Society 111 (2011): 3667-3668. Web.

32. Mayer, Kathryn, and Jason Hafner. "Localized Surface Plasmon Resonance Sensors." *Chemical Reviews*, American Chemical Society 111 (2011): 3828-3857. Web.

33. Zhang, Qiang et al. "Facile Synthesis of Ag Nanocubes of 30 to 70 nm in Edge Length with CF_3COOAg as a Precursor." *Chemistry* 16(33) (2010): 10234-10239. Web.

34. Verschuuren, Marcus Antonius. "Substrate Conformal Imprint Lithography for Nanophotonics." Diss. Utrecht University, 2010. Print.

35. Hong, Young-Kyu et al. “Controlled two-dimensional distribution of nanoparticles by spin-coating method.” *Applied Physics Letters*, Vol. 80, Nr. 5 (2002): 844-846. Web.

36. *File: Surface Acoustic Wave Sensor Interdigital Transducer Diagram.png*. Wikimedia Commons, Aug. 19, 2012. Accessed Nov. 12, 2013. http://commons.wikimedia.org/wiki/File:Surface_Acoustic_Wave_Sensor_Interdigitated_Transducer_Diagram.png.

37. Bouatra S, Aziat F, Mandal R, Guo AC, Wilson MR, et al. (2013) *The Human Urine Metabolome.* PLoS ONE 8(9): e73076. doi:10.1371/journal.pone.0073076.

38. Wong Cintyu and Joel Burgess. “Modifying the Surface Chemistry of Silica Nano-Shells for Immunoassays.” *Journal of Young Investigator* (2002). Web.

39. Anderson, Nicole S. et al. “Urinary levels of Bcl-2 are elevated in ovarian cancer patients.” *Gynecologic Oncology* 112 (2009): 60-67. Web.

APPENDICES

Appendix A Additional Information

Most of the information provided in this thesis has been provided with the visual proof of the image from which the quantitative numbers came. There are two exceptions for this. One is the data from Figure 3-8 and Figure 3-9. This was excluded from the main paper because the number of image is extremely high and a selection of images will be included. The other images excluded were the control images from micro-mixing. There were also a lot of these images for the control group, and they will also be provided.

As the number of images for the data in Figures 3-8 and 3-9 are extremely high, only some of the images will be shown by placing the MEF image next to the control image at the same concentrations.

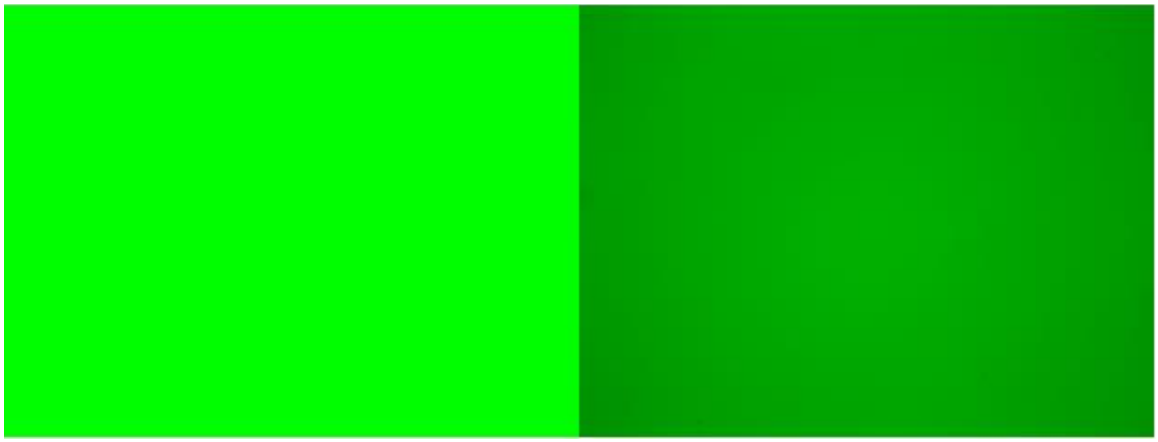

Figure A-1. Detection of 10,000 ng/mL. MEF is on the left, and the control is on the right.

In Figure A.1, it is difficult to get an idea of the amount of enhancement because the MEF side of the figure is basically the same as for a concentration of 1,000 ng/mL. The best way to truly evaluate this concentration would be to lower the exposure of the camera. However, in this work, it is of more interest to evaluate nanogram levels. These high concentrations are just to show that the work is consistent.

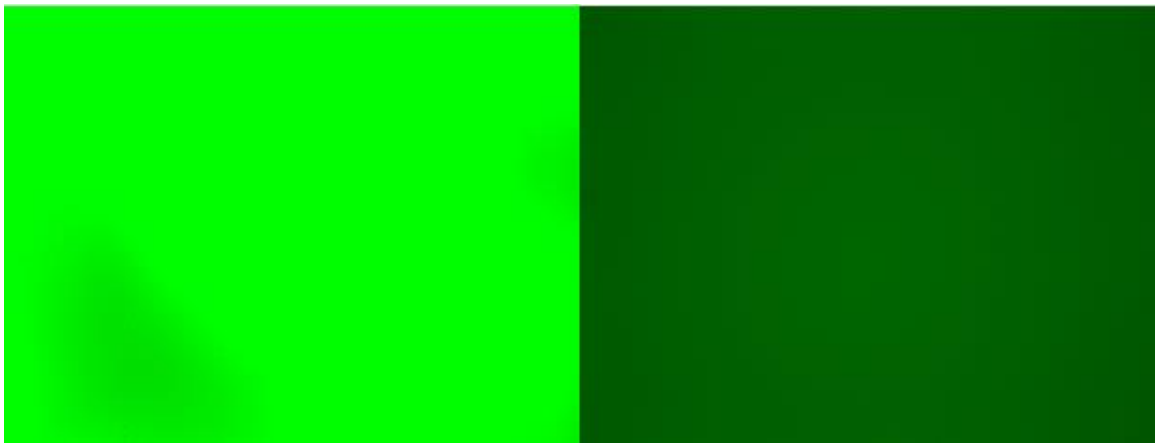

Figure A-2. Detection of 5,000 ng/mL. MEF is on the left, and the control is on the right.

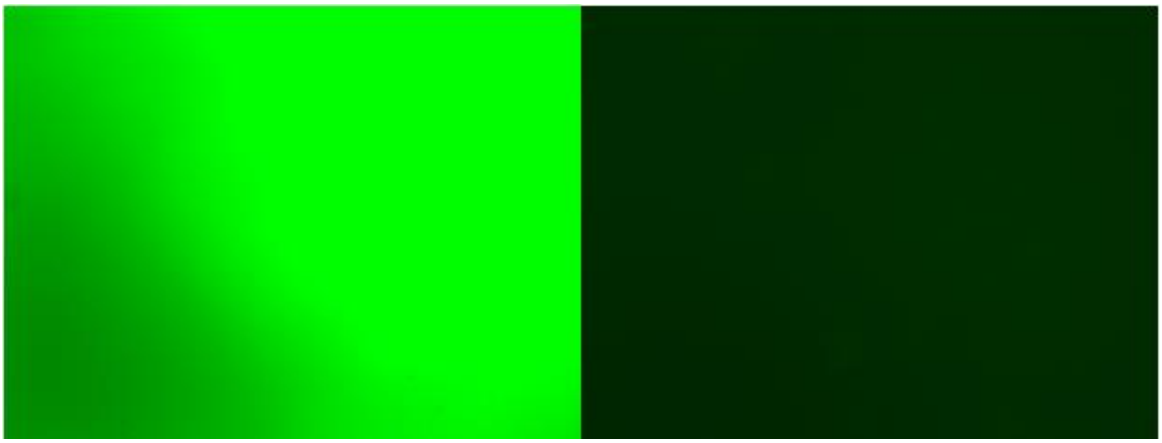

Figure A-3. Detection of 1,000 ng/mL. MEF is on the left, and the control is on the right.

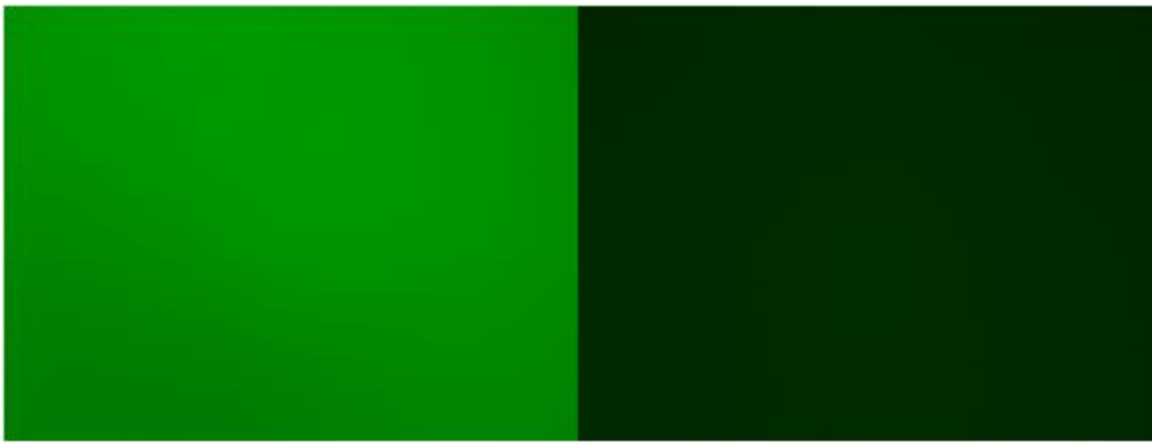

Figure A-4. Detection of 500 ng/mL. MEF is on the left, and the control is on the right.

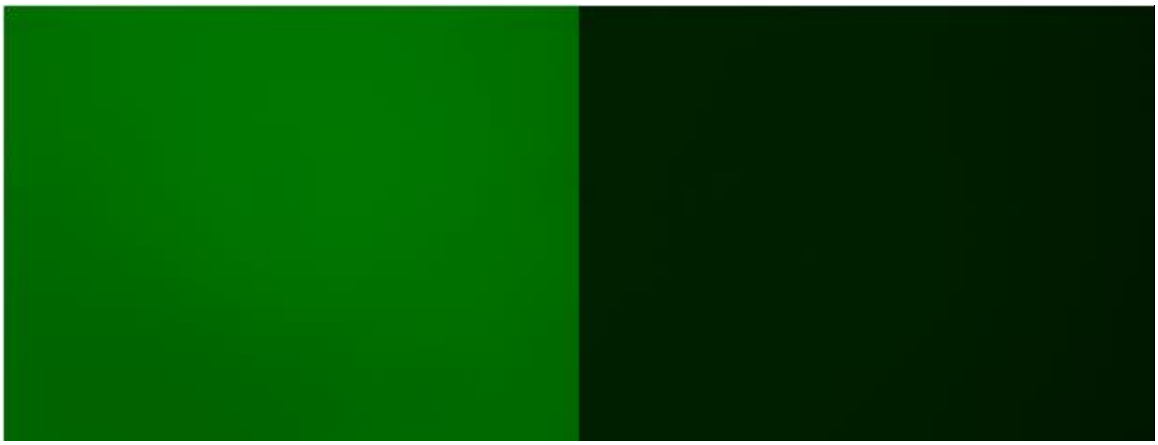

Figure A-5. Detection of 300 ng/mL. MEF is on the left, and the control is on the right.

At this point, all of the control images begin to look like the control figure from Figure A.4 and Figure A.5. Therefore, from this point on in Appendix A, MEF images will be shown compared to MEF images at different concentrations.

Figure A-6. MEF detection at concentrations just below control detection capability. 100 ng/mL on the left, 60 ng/mL in the center, and 30 ng/mL to the left.

Figure A-7. MEF detection at concentrations far below control detection capability. 10 ng/mL on the left, 2 ng/mL in the center, and 0 ng/mL to the left.

The last image to be included in Appendix A, are the control group images from the micro-mixing experiment. These images were used in making Figures 5-1 and 5-3 and can be compared with the images in Figure 5-2 if so desired.

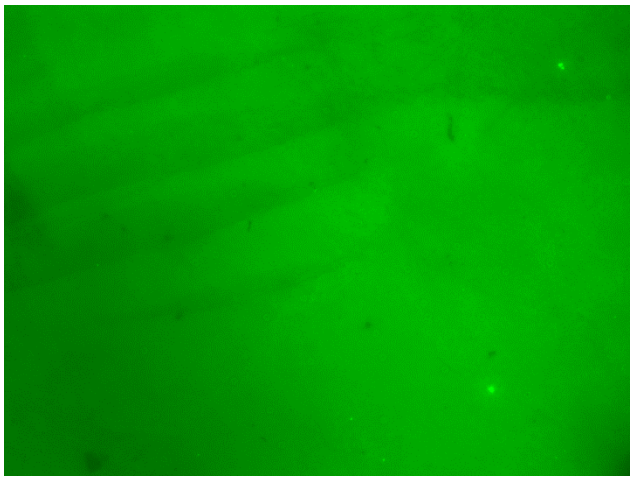

Figure A-8. Incubation without micro-mixing for 30 minutes.

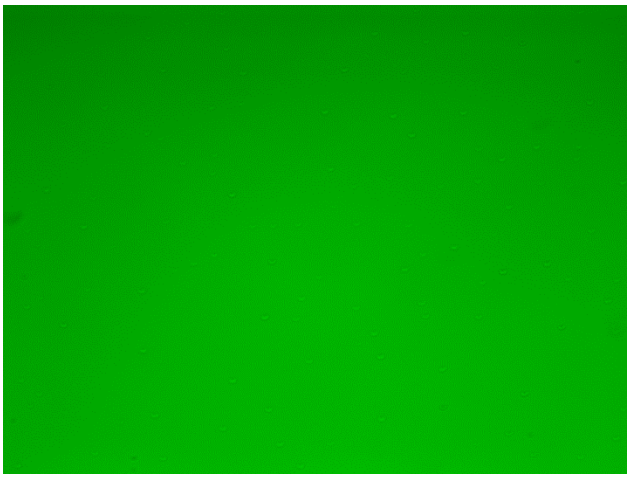

Figure A-9. Incubation without micro-mixing for 1 hour.

As was noted in Chapter 5, there is not much difference between incubating for 30 minutes versus 1 hour. Image analysis is required to measure the difference which was done in Chapter 5.

Appendix B Codes Used in Simulations

In this section, complete codes used in simulations with FDTD Solutions will be shown as will images that may be helpful in understanding how this simulation was set up. In Figure A.2-1, a screen shot of the simulation setup is provided.

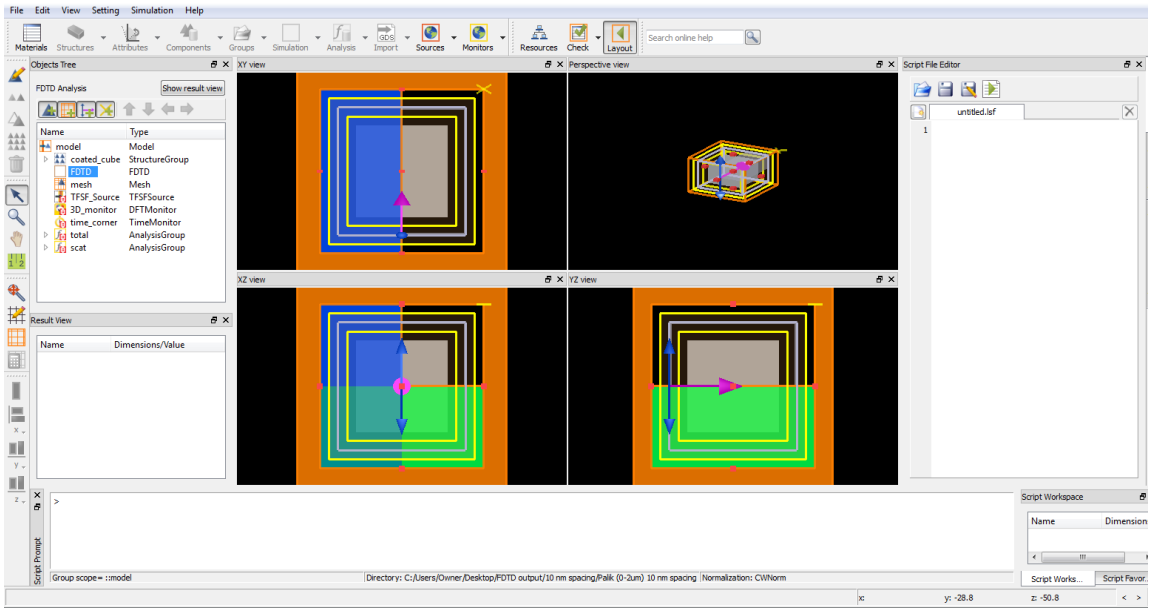

Figure B-1. Screenshot of FDTD Solutions setup.

With this setup, the code below was used for calculating the absorption, scattering, and extinction spectra:

```
runanalysis;
Cube = 1; # set 0 to not perform this test, 1 to perform the
test
Tri = 0; # set 0 to not perform this test, 1 to perform the test
Sph = 0; # set 0 to not perform this test, 1 to perform the test
f=getdata("total","f"); # get freqency data
lambda=c/f*1e9;
sigmascat = getdata("scat","sigma");
sigmaabs = -getdata("total","sigma");
sigmaext=sigmaabs+sigmascat;
if(Sph) {
ri= getnamed("coated_sphere","r"); # the radius of the inner
sphere
th= getnamed("coated_sphere","h_coating");
aeff= ri+2*th;
}
```

```
if(Cube) {
li= getnamed("coated_cube", "side");
th= getnamed("coated_cube", "h_coating");
xx = li + 2*th;
aeff=((3*(xx^3))/(4*pi))^0.33333;
}
if(Tri) {
li= getnamed("coated_pyr","x span");
z= getnamed("coated_pyr","z span");
th= getnamed("coated_pyr", "h coating");
base = li+2*th;
ht = z+2*th;
v=(base*base)*ht/3;
aeff=((3*v)/(4*pi))^0.33333;
}
Qabs=sigmaabs/(pi*aeff^2);
Qscat = sigmascat/(pi*aeff^2);
Qext=Qabs+Qscat;
write("Cube50nm_AgPd_C50nmS0nm.txt",num2str([lambda, Qabs,
Qscat, Qext]));
plot(lambda,Qabs,Qscat,Qext,"wavelength (nm)", "Intensity");
     legend("Absorption","Scattering","Extinction");
```

This code results in the absorption, scattering, and extinction data. The other cases simulated which were not shown in Chapter 3.4 are available in the following figures which range from 10 to 90 nm.

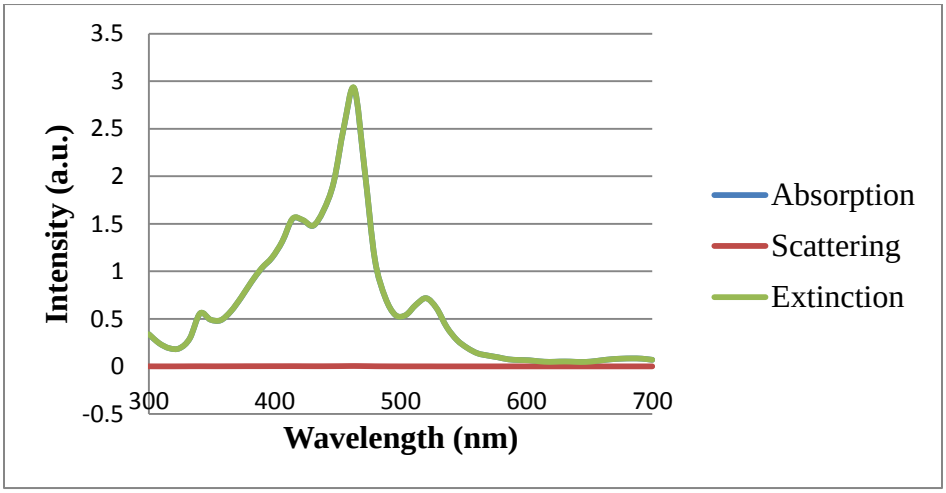

Figure B-2. Spectra of nanocube with 10 nm edges.

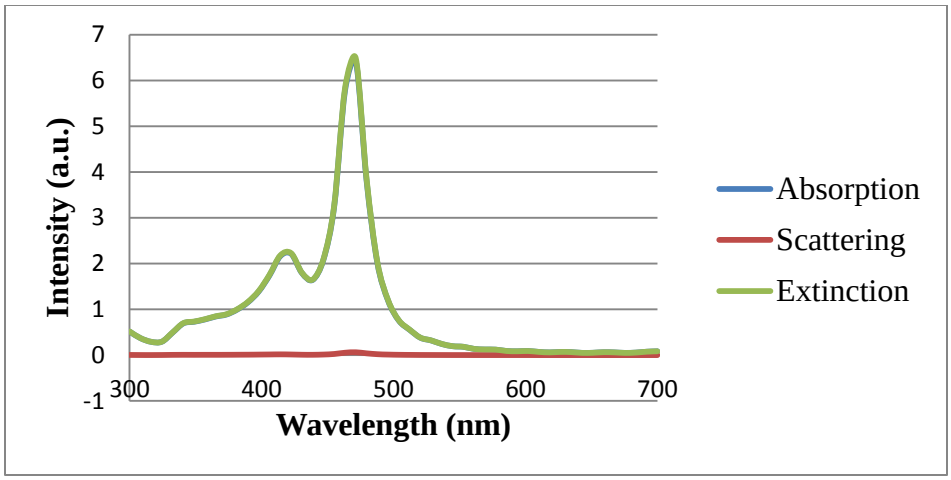

Figure B-3. Spectra of nanocube with 15 nm edges.

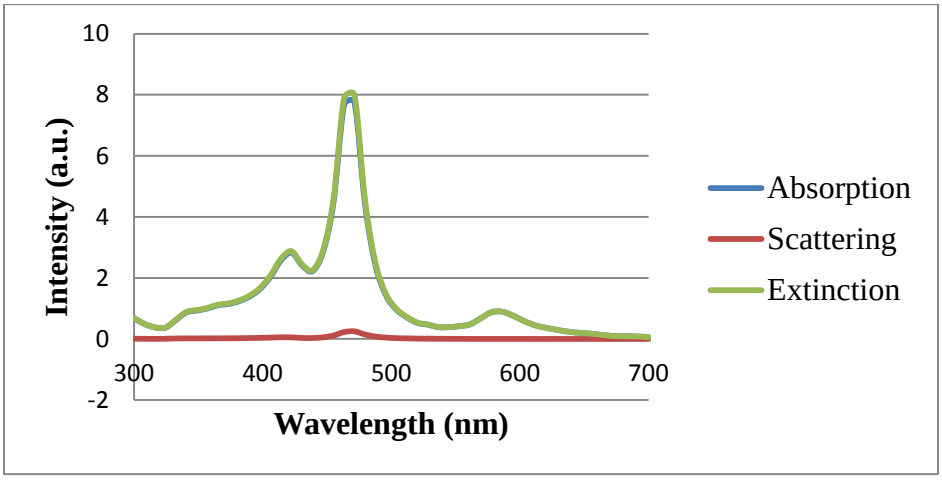

Figure B-4. Spectra of nanocube with 20 nm edges.

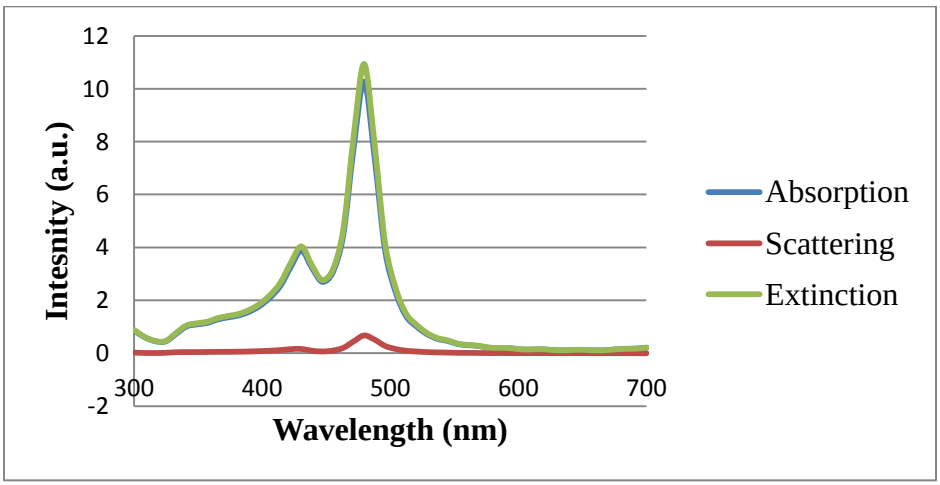

Figure B-5. Spectra of nanocube with 25 nm edges.

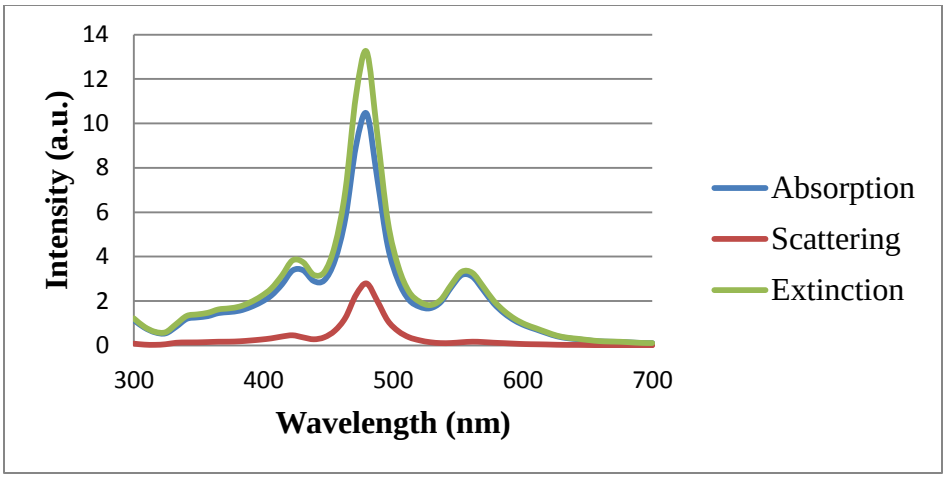

Figure B-6. Spectra of nanocube with 35 nm edges.

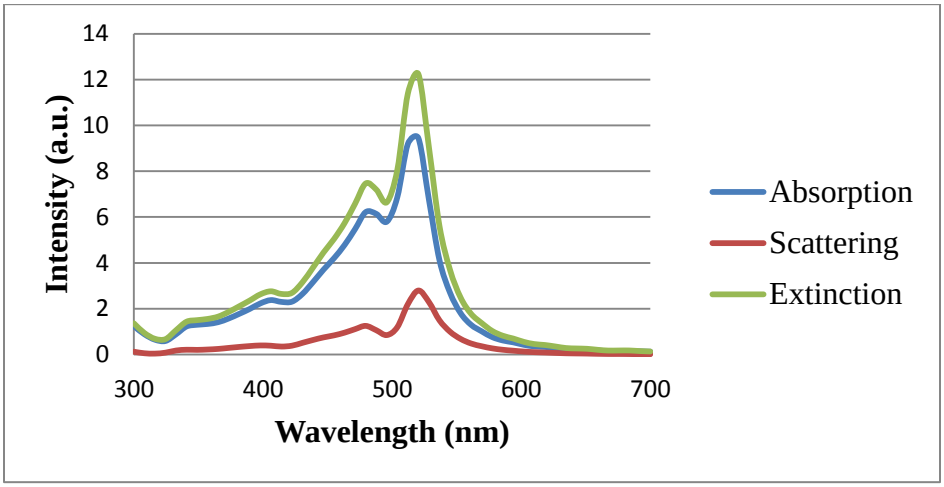

Figure B-7. Spectra of nanocube with 40 nm edges.

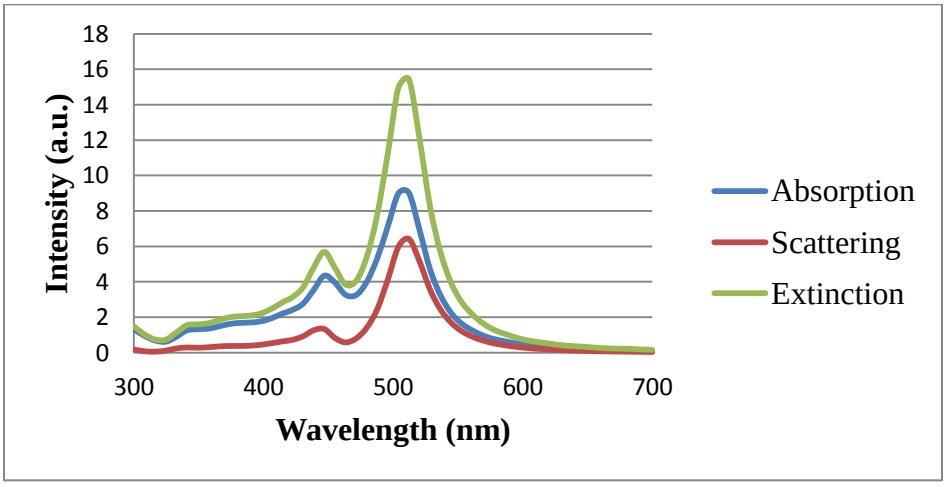

Figure B-8. Spectra of nanocube with 45 nm edges.

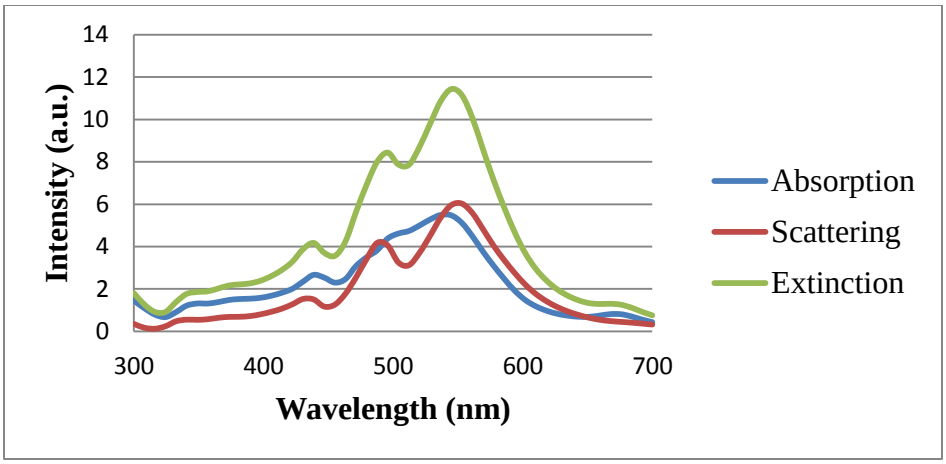

Figure B-9. Spectra of nanocube with 60 nm edges.

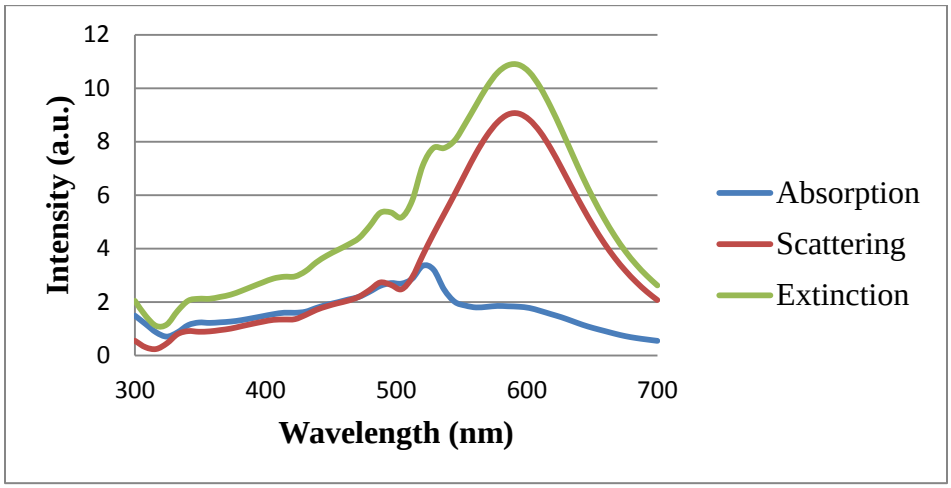

Figure B-10. Spectra of nanocube with 80 nm edges.

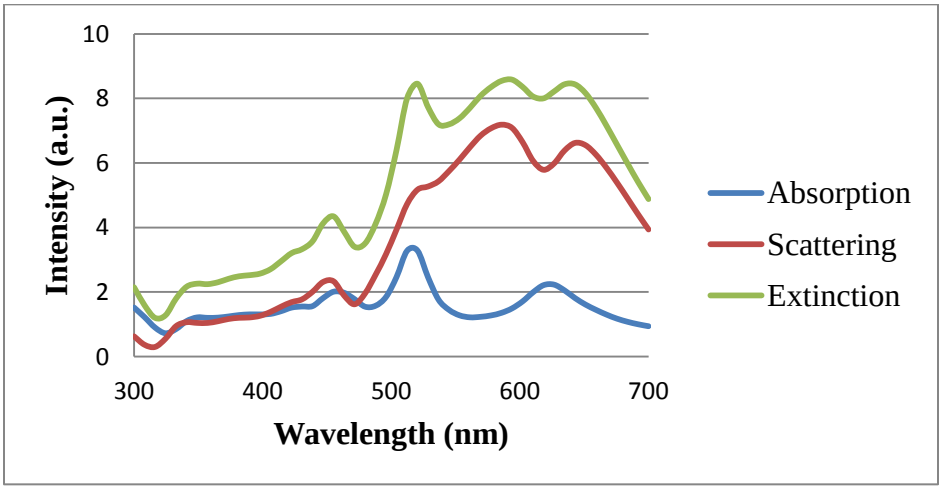

Figure B-11. Spectra of nanocube with 90 nm edges.

Appendix C Optimization Progress

There are plenty of different aspects of this research currently being optimized. For now, the focus has been on optimizing the MEF aspect of the research to be able to reach detection limit below 1 ng/mL. The first step to attempt for this research has been to deposit SiO_2 on top of the silver nanoparticles. The reason we believe this could improve the enhancement is not only because the SiO_2 will reduce oxidation, but it will red-shift the refractive index bringing it closer to 488 nm. It will also ensure that no fluorophore gets in too close proximity to nanoparticles, which will result in quenching.

So far, the deposition of SiO_2 has been done, but the actual MEF experiments have not been completed yet. The deposition was done in a Level 1000 cleanroom using an RIE/RFPE control system from Plasma Therm. The deposition took 26 seconds and included 500 cm^3 of N_2O and 11 cm^3 of SiH_4 with a wall temperature of 60 °C. This resulted in a 12 nm layer of SiO_2 on top of the nanoparticles.

Others in the group are currently working on improving removal. So far, this includes different power supplies, different time frames, and different IDT designs. Mixing is currently the most consistent aspect of the research so optimization there is not currently as high of a priority.